yet complete; for example, there is no information about cell-cycle progression in cells expressing mutant ORC with reduced ATPase. Furthermore, a mutation may affect activities other than the one targeted, and so analyses with multiple mutants are necessary to understand the exact role of the targeted activity.

Orc1p belongs to the AAA$^+$ (ATPases associated with a variety of cellular activities) family of proteins [30]. AAA$^+$ proteins have several consensus domains [30], and the Walker B motif and the sensor 1 and 2 regions are thought to be important for ATPase activity [31,32]. X-ray structural analysis of the *E. coli* HslU (heat-shock locus U) protein, which belongs to AAA$^+$ family, showed that Arg^{393}, a conserved arginine residue in the sensor 2 region, can interact with the γ-phosphate of ATP [33]. It is thought that the sensor 1 and 2 regions detect the status of ATP versus ADP in the nucleotide-binding site and regulate ATPase activity [32].

In the present study we searched Orc1p for essential amino acid residues located in the sensor 1 and 2 regions. Analyses *in vivo* and *in vitro*, with mutant ORC with reduced ATPase activity, suggest that ORC's ATPase activity is involved in MCM loading on to origin DNA.

EXPERIMENTAL

Materials

[α-^{32}P]ATP (3000 Ci/mmol) and [γ-^{32}P]ATP (6000 Ci/mmol) were from Wako Pure Chemical Industries and GE Healthcare respectively. Wild-type ORC, ORC-1A [ORC containing mutant Orc1p with defective Walker A motif (GXXGXGK^T/$_S$)] and ORC-1R [ORC with Orc1R694Ep (Orc1p Arg^{694}→Glu mutant)] were expressed in Sf9 [*Spodoptera frugiperda* (fall armyworm)] insect cells infected with recombinant baculoviruses and were purified as described previously [19]. A recombinant baculovirus for ORC-1A was donated by Professor Stephen P. Bell, Howard Hughes Medical Institute, Department of Biology, Massachusetts Institute of Technology, Cambridge, MA, U.S.A. DNA fragments (290 bp) containing wild-type *ARS1* (autonomously replicating sequence 1) mutant *ars1* (A$^-$B1$^-$) were prepared by PCR as described previously [34] and purified by PAGE. DNA fragments were radiolabelled with T4 polynucleotide kinase and [γ-^{32}P]ATP. The specific radioactivity of each probe was about 4000 c.p.m./fmol of DNA.

Strains, plasmids and medium

S. cerevisiae strains used in the present study are shown in Supplementary Table S1 at http://www.BiochemJ.org/bj/413/bj4130535add.htm. Yeast strain SKY007a [35] was a gift from Dr Katsuhiko Shirahige (Tokyo Institute of Technology, Tokyo, Japan) or Dr Yuji Hori (Japan Tobacco Inc., Tokyo, Japan), and DK186 [36] was a gift from Dr Douglas R. Kellogg (Department of Molecular, Cell and Developmental Biology, University of California Santa Cruz, Santa Cruz, CA, U.S.A.).

Plasmids pRS405-GAL1-10-ORC2,5, pRS404-GAL1-10-ORC3,4 and pRS403-GAL1-10-ORC1,6 were donated by Professor Stephen Bell [27]. DNA inserts were transferred to pRS413 [*HIS3* (imidazoleglycerol-phosphate dehydratase gene)], pRS414 [*TRP1* (phosphoribosylanthranilate isomerase gene)] and pRS415 [*LEU2* (β-isopropylmalate dehydrogenase gene)] [37] to construct pRS413-GAL1-10-ORC2,5, pRS414-GAL1-10-ORC3,4 and pRS415-GAL1-10-ORC1,6.

ORC1 sequences were ligated into the XbaI–SacI region of pMM19 (a pUC19 derivative with chloramphenicol resistance instead of ampicillin resistance) and used for PCR-based site-directed mutagenesis. The pMM19 derivatives with *ORC1*, *orc1N600A*, *orc1N600T*, *orc1R694A*, *orc1R694E* or *orc1R704E* were named pMM-100–pMM-105 respectively. These *orc1* sequences were then inserted into XbaI–SacI region of YCplac22 (a low-copy-number plasmid containing the *TRP1* gene) [38] and the derivatives were named pHT-100–pHT-105 respectively. In addition, the *ORC1* gene in pRS415-GAL1-10-ORC1,6 (pMT-100) was replaced with each mutant *orc1* gene from pMM-101 to -105, and the derivatives were named pMT-101–pMT-105 respectively.

GAL1 (galactokinase gene) was ligated into the BamHI–EcoRV region of pRS413 to construct pRS413-GAL1. Wild-type *HA-ORC1* was constructed by inserting synthetic oligonucleotides encoding the HA (haemagglutinin) epitope immediately upstream of the initiation ATG codon of *ORC1*, and this DNA fragment was ligated into the EcoRV–XhoI region of pRS413-GAL1 to construct pRS413-GAL1-HA-ORC1. Wild-type *ORC1* genes in pRS413-GAL1-ORC1 were replaced with *orc1R694E* in pHT-104. pRS413-GAL1-HA-orc1K485T was constructed using a QuikChange® Site-Directed Mutagenesis Kit (Stratagene) and pRS413-GAL1-ORC1 as template.

Cells were cultured at 30 °C in SC (synthetic complete) medium with appropriate amino acid depletion, or in YP medium (2 % Bacto peptone, 1 % Bacto Yeast Extract and 150 μg/ml adenine hemisulfate) with 2 % glucose, 2 % raffinose or 2 % galactose.

Modifications of the *MCM4* gene with the 13Myc epitope was performed as described previously [39]. PCR was performed using pFA6a-13Myc-TRP1 plasmid as a template and primers containing DNA sequences for the C-terminal region of the *MCM4* gene. The amplified DNA was transformed into strain DK186. The construct of the resultant strain (yMT50) was confirmed by the colony PCR method.

Plasmid shuffling

Plasmids (pHT-100, -101, -102, -103, -104 or -105) were transformed into SKY007a by the lithium acetate method. The transformant was selected on SC agar plates, containing 5-FOA (5-fluoro-orotic acid), but without tryptophan.

Filter-binding assay for ATP binding to ORC

This was performed as described previously [21], but with some modifications. ORC was incubated with [α-^{32}P]ATP at 30 °C for 5 min in 40 μl of buffer T [25 mM Tris/HCl, pH 7.6, 5 mM $MgCl_2$, 70 mM KCl, 5 mM dithiothreitol and 5 % (v/v) glycerol]. In some experiments, ORC was further incubated with DNA fragments at 30 °C for 5 min in the same buffer. Samples were passed through nitrocellulose membranes (Millipore HA; 0.45 μm pore size) and washed with ice-cold buffer T. The radioactivity remaining on the filter was monitored with a liquid-scintillation counter.

Gel-electrophoretic mobility-shift assay for DNA binding to ORC

This was performed as described previously [34]. ORC was pre-incubated with adenine nucleotides for 5 min at 30 °C, and further incubated with radiolabelled DNA fragments (100 fmol) for 5 min at 30 °C in 10 μl of buffer T containing 2 mg/ml BSA and 40 μg/ml poly(dI/dC) (non-specific competitors). The reaction sample was loaded on to a 3.5 %-(w/v)-polyacrylamide gel containing 0.045 M Tris/borate (pH 8.3) and 1 mM EDTA. The gel was electrophoresed for 1.5 h at 200 V, dried, and autoradiographed.

Assay for the ATPase activity of ORC

The ATPase activity of ORC was measured as described previously [19], with some modifications. ORC (0.3 pmol) was incubated with DNA fragments (6 pmol) in 10 μl of ATPase buffer (50 mM Hepes/KOH, pH 7.6, 150 mM KCl, 5 mM magnesium acetate, 1 mM EDTA, 1 mM EGTA, 0.02 % Nonidet P40 and 10 μM radiolabelled ATP) for 60 min at room temperature (25 °C). The reaction was stopped by addition of 2 % (w/v) SDS (5 μl) and adenine nucleotides were separated on polyethyleneimine–cellulose F TLC plates (Merck).

Filter-binding assay for DNA binding to ORC

This was performed as described previously [20], with some modifications. ORC (0.2 pmol) was incubated with ATP for 5 min at 30 °C in 40 μl of buffer T, and further incubated with radiolabelled DNA fragments at 30 °C for 5 min in the same buffer. Samples were passed through nitrocellulose membranes (Millipore HA; 0.45 μm pore size) and washed with ice-cold buffer T. The radioactivity remaining on the filter was monitored with a liquid-scintillation counter.

FACS analysis

Samples were prepared as previously described [41], with some modifications. Cells were pelleted by centrifugation (20000 *g* for 1 min), washed with sterilized water, and fixed in 70 % (v/v) ethanol for 12 h. Cells were again pelleted, re-suspended in 50 mM sodium citrate, pH 7.4, sonicated (Cultra 5 homogenizer; Taitec, Saitama, Japan; power setting 7 W) for 1 min, treated with 0.25 mg/ml RNase A for 1 h at 50 °C, and then with 1 mg/ml Proteinase K for 1 h at 50 °C. DNA was stained with 50 μg/ml of propidium iodide, and 20000 cells from each sample were scanned with a FACSCalibur flow cytometer (Becton Dickinson).

Immunoblotting

Yeast spheroplasts were lysed with Triton X-100, and samples were processed into soluble (supernatant) and chromatin (insoluble precipitate) fractions by centrifugation (20000 *g* for 1 min) as previously described [41]. Equivalent amounts (total protein) of fractions were electrophoresed on 7.5 or 10 % (w/v) polyacrylamide gels containing 0.1 % SDS, transferred to PVDF membrane, and probed with monoclonal antibodies 12CA5, SB3, Mcm2-18, Mcm3-28 and 9E10 against HA, Orc3p, Mcm2p (MCM protein 2p), Mcm3p and Myc respectively, which were donated by Dr Bruce Stillman (Cold Spring Harbor Laboratory, Cold Spring Harbor, NY, U.S.A.) [31,34,41].

ChIP (chromatin immunoprecipitation) assay

The ChIP assay was performed as described in [42], with some modifications. Cells were cross-linked with 1 % formaldehyde for 15 min at 25 °C. After addition of 125 mM (final concn.) glycine, cells were harvested and lysed with glass beads in buffer (50 mM Hepes/KOH, pH7.5, 140 mM NaCl, 1 mM EDTA, 1 % Triton X-100, 0.1 % sodium deoxycholate, 1 mM PMSF, 2 mM benzamidine, 1 μg/ml leupeptin and 2 μg/ml pepstatin A). Samples were sonicated 30 times for 10 s each (an average fragment size of 0.5–1 kb). Immunoprecipitation was performed with magnetic beads, which were coated with Protein G (Dynal) and antibody against Orc3p (SB3) or Myc (9E10). Precipitates were washed, processed for DNA purification and subjected to PCR. In PCR cycles, an initial denaturation of 0.5 min at 95 °C was followed by 35 cycles with denaturation for 0.5 min at 95 °C, annealing for 0.5 min at 50 °C, polymerization for 1 min at 72 °C, and a final extension for 4 min at 72 °C. The PCR products were separated by 3%-(w/v)-agarose-gel electrophoresis and visualized under UV light after ethidium bromide staining.

RESULTS AND DISCUSSION

Identification of essential amino acid residues in the sensor 1 and sensor 2 regions of Orc1p

In the AAA$^+$ family of proteins, the amino acids thought to be important for the ATPase activity are asparagine and threonine residues in the sensor 1 region, and basic amino acid residues in the sensor 2 region [30]. We searched for these amino acid residues in *S. cerevisiae* Orc1p, and found that Asn^{600} in the sensor 1 region, and Arg^{694} and Arg^{704} in the sensor 2 region, are conserved among Orc1ps from various species. Arg^{694} and Arg^{704} correspond to Arg^{208} and Arg^{215} of *E. coli* clamp loader (another AAA$^+$ protein) [30], and these residues recognize the γ-phosphate group of bound ATP [43].

To examine the roles of these amino acids, we used site-directed mutagenesis to create five mutant *orc1* genes (*orc1N600A*, *orc1N600T*, *orc1R694A*, *orc1R694E* and *orc1R704E*). Each mutant gene was inserted into a plasmid (YCplac22) that contains the *TRP1* gene. The plasmid was transformed into strain SKY007a, which contains a chromosomal *ORC1* gene deletion and an alternative wild-type *ORC1* gene in a plasmid with the *URA3* (uracil-biosynthesis gene) selectable marker (pKS007) [35]. When the transformant was grown on agar plates containing 5-FOA, the *URA3*-containing plasmid was selected against and lost, causing cells to rely solely on the mutant *orc1* gene (plasmid shuffling).

As shown in Figure 1, 5-FOA inhibited growth of cells expressing Orc1N600Ap, suggesting that Asn^{600} is essential for cell growth. This defect may be related to the ATPase activity of Orc1p, because cells expressing Orc1N600Tp grew normally (Figure 1) (see above). 5-FOA also inhibited growth of cells expressing Orc1R694Ap, Orc1R694Ep and Orc1R704Ep, showing that Arg^{694} and Asn^{704} are also essential.

We then examined the effect of overexpression of mutant Orc1p on the growth of the wild-type strain. At first, not only mutant Orc1p, but also the other five subunits, of ORC were overexpressed using a galactose-dependent expression system (the *GAL1-10* promoter). As shown in Figure 2, cells with plasmid that contains *orc1R694A* or *orc1R694E* under the *GAL1-10* promoter, showed a growth defect in the presence of galactose, but not with glucose, suggesting that overexpression of Orc1R694Ap or Orc1R694Ep causes a growth defect. Cells with plasmid that contained *orc1N600A*, *orc1N600T* or *orc1R704E* grew normally (Figure 2). Overexpression of Orc1R694Ap or Orc1R694Ep alone also caused a similar growth defect (results not shown).

As described above, the growth defect caused by overexpression of mutant ORC with reduced ATPase activity (ORC with Orc1D569Yp or with Orc1D569Fp) is suppressed by simultaneous overexpression of Cdc6p [27]. Overexpression of Cdc6p did not suppress the growth defect caused by Orc1R694Ap or Orc1R694Ep (results not shown), suggesting that this defect is not due to titration of Cdc6p, but to the inability of mutant ORC to complete one of the steps in DNA replication.

Biochemical characterization of ORC-1R

We termed ORC with Orc1R694Ep 'ORC-1R' and purified both ORC-1R and wild-type ORC from Sf9 insect cells overexpressing each type of ORC. As shown in Figure 3(A), both were prepared to similar purity, and no apparent degradation of subunits was observed.

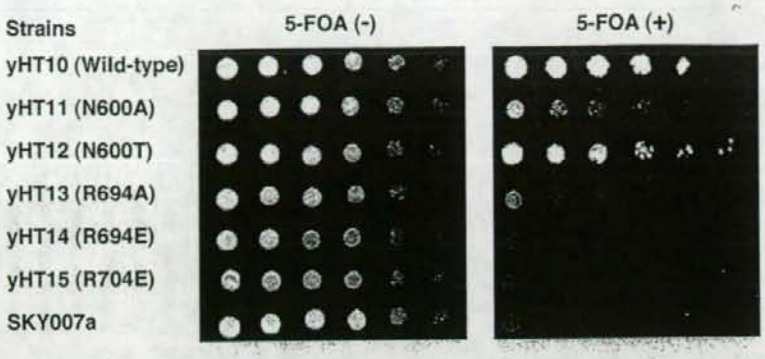

Figure 1 Identification of the amino acid residues of Orc1p that are essential for cell growth

Cell suspensions [left to right, 4-fold serial dilution of a suspension with an attenuance (D_{600}) of 4.0] of strain-SKY007a derivatives with expression plasmids for wild-type Orc1p, Orc1N600Ap, Orc1N600Tp, Orc1R694Ap, Orc1R694Ep or Orc1R704Ep (yHT10–yHT15 respectively) were spread on SC/agar plates with or without 0.1% 5-FOA and incubated at 30°C for 2 days. Similar results were obtained in two independent experiments.

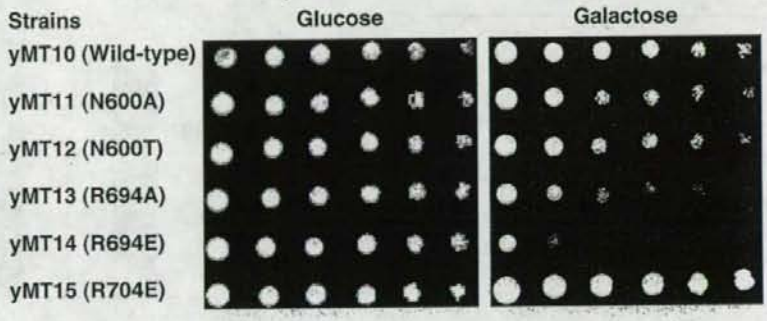

Figure 2 Cell growth defect caused by overexpression of mutant ORC

Cell suspensions (left to right; 4-fold serial dilutions of a suspension with a D_{600} of 1.0) of strain-yMT01 derivatives with expression plasmids for the wild-type Orc1p, Orc1N600Ap, Orc1N600Tp, Orc1R694Ap, Orc1R694Ep or Orc1R704Ep (yMT10–yMT15 respectively) were spread on SC/agar plates with 2% glucose, or 2% both raffinose and galactose, and incubated at 30°C for 2 days. Similar results were obtained in two independent experiments.

ATP binding was compared using a filter-binding assay. Similar amounts of ATP bound to both ORC-1R and wild-type ORC (Figure 3B). Scatchard-plot analysis showed that the K_d values, and the amounts of bound ATP per ORC, were virtually indistinguishable between ORC-1R and wild-type ORC (Figure 3C). The K_d values for wild-type ORC and ORC-1R were 2.7 and 2.9 nM respectively. These results suggest that the mutation did not affect ATP binding and, therefore, that the ATPase activity of ORC-1R can be measured by the standard method (see below).

It has been reported that origin DNA fragments can stimulate ATP binding to Orc1p [19,21]. We therefore examined the effect of origin (*ARS1*) DNA fragments on ATP binding to ORC-1R. As shown in Figure 3(D), *ARS1* DNA fragments increased the amount of ATP bound to wild-type ORC, as reported previously [21]. ORC-1R gave similar results, suggesting that the R694E mutation affects neither ATP binding to Orc1p nor the effect of DNA on the ATP-binding.

Origin DNA binding to ORC and ORC-1R was also studied by using radiolabelled DNA and the filter-binding assay. As shown in Figure 4(A), the DNA-binding activities were indistinguishable. *ARS1* contains four elements (A, B1, B2 and B3) important for its origin function [44], among which A and B1 are ORC-binding sites [17,45]. We examined the extent of binding of each ORC to radiolabelled wild-type *ARS1* or mutant *ars1* (A^-B1^-) DNA fragments in the presence of various concentrations of poly(dI/dC), a non-specific competitor DNA (Figure 4B). Wild-type ORC and ORC-1R both bound to wild-type *ARS1* more efficiently than to mutant *ars1*, suggesting that the mutation R694E did not affect the specificity of ORC binding to origin DNA. The fact that ORC-1R had defective ATPase activity (see below), but still bound DNA normally, suggests that the ATPase activity of ORC is not involved in ORC binding to origin DNA (this is the first quantitative analysis of the DNA-binding activity of mutant ORC with reduced ATPase activity).

We also compared the DNA-binding properties of ORC-1R and wild-type ORC by a gel-electrophoretic mobility-shift assay. As shown in Figure 4(C), wild-type ORC bound to wild-type *ARS1*, but not mutant *ars1* fragments, in the presence of ATP, but did not bind to any DNA fragments in the presence of ADP or in the absence of adenine nucleotides. These results are consistent with a previous report [20]. Similar results were observed with ORC-1R, suggesting that the mutation in Orc1p did not affect the DNA-binding properties of ORC.

Finally, we measured the ATPase activity of ORC-1R. As shown in Figure 5, wild-type ORC showed the same level of ATPase activity as reported previously, and ORC-1A showed no

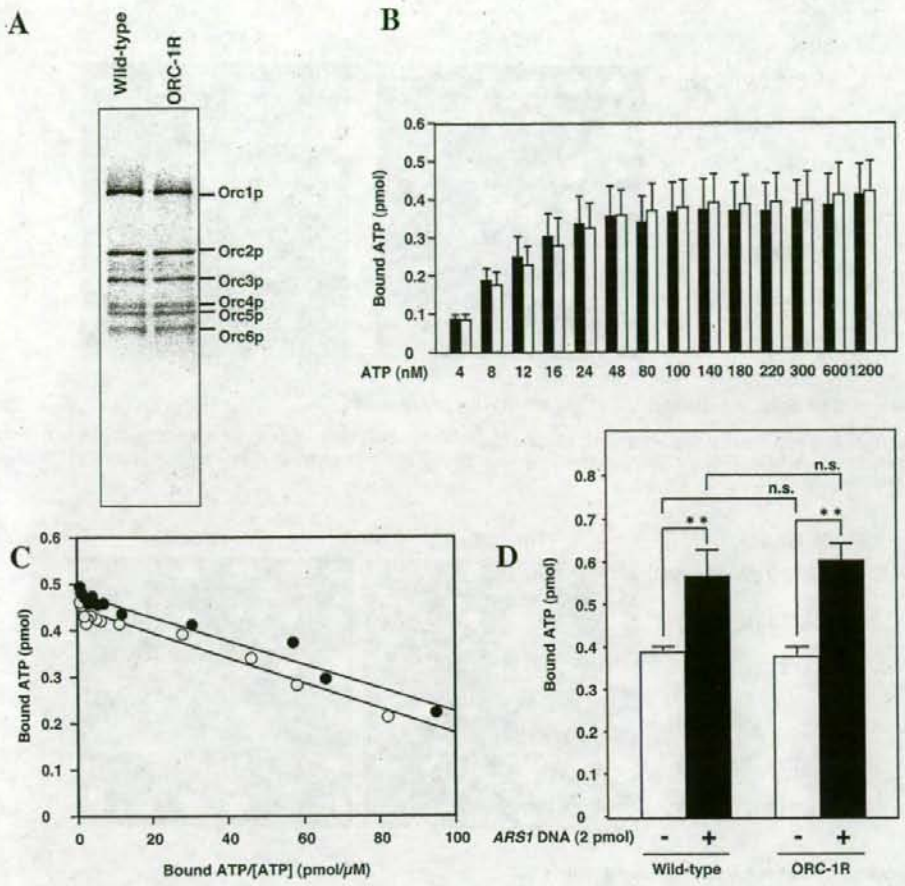

Figure 3 ATP-binding activity of ORC-1R

Wild-type ORC and ORC-1R were purified from Sf9 insect cells co-infected with viruses expressing all six *ORC* genes. (**A**) Wild-type ORC and ORC-1R (1 pmol) were separated by SDS/10 %-(w/v)-PAGE and subsequently analysed by silver staining. Similar results were obtained in two independent experiments. (**B**) Portions (1 pmol) of wild-type ORC (black bars) or ORC-1R (white bars) were incubated with radiolabelled ATP as indicated, and ATP attached to ORC was determined by the filter-binding assay. Values are means ± S.D. ($n = 3$). (**C**) Scatchard-plot analysis of data from (**B**). (**D**) Samples as described in (**B**) were first incubated with 5 μM radiolabelled ATP, then incubated with or without *ARS1* DNA fragments. ATP attached to ORC was determined by the filter-binding assay. Values are means ± S.D. ($n = 3$). $^{**}P < 0.01$; n.s., not significant.

ATPase activity, again as reported previously [19]. The ATPase activity of ORC-1R was about half that of wild-type ORC (Figure 5), showing that the R694E mutation in Orc1p reduces ATPase activity, and that the sensor 2 region is important for the ATPase activity. As described above, Arg^{694} of Orc1p corresponds to Arg^{208} of the *E. coli* clamp loader protein [30], which recognizes the γ-phosphate group of ATP [43]. Likewise, Arg^{694} in Orc1p may recognize the γ-phosphate group of ATP bound to the Walker A motif and stimulate hydrolysis.

It has been reported that double-stranded *ARS1* DNA fragments inhibit the ATPase activity of ORC [19]. In the present study we examined the effect of wild-type *ARS1* and mutant *ars1* (A^-B1^-) DNA fragments on the ATPase activity of ORC-1R. Wild-type *ARS1*, but not mutant *ars1* DNA fragments, inhibited the ATPase activity of wild-type ORC (Figure 5). Similar results were observed with ORC-1R, suggesting that the R694E mutation did not affect the origin DNA-dependent regulation of ORC ATPase activity. Thus ORC-1R shows reduced ATPase activity both in the presence and in the absence of origin DNA.

Effect of overexpression of Orc1R694Ep on pre-RC formation and on cell-cycle progression

To understand the role of ORC ATPase in cells, we examined the effect of overexpression of Orc1R694Ep on pre-RC formation and on cell-cycle progression. Yeast strains yMT40 and yMT44 have plasmids with GAL1-HA-ORC1 and GAL1-HA-orc1R694E respectively. We examined the effect of this on the loading of MCM on to chromatin. Cells synchronized at G2/M phase were incubated with galactose to overexpress each type of Orc1p and were then released into fresh medium containing α-factor (a yeast mating pheromone) (Figure 6A). As shown in Figures 6(B) and 6(C), loading of Mcm2p, Mcm3p and Mcm4p was less efficient in strain yMT44 than in strain yMT40, suggesting that overexpression of Orc1R694Ep inhibited MCM loading on to chromatin, thus inhibiting pre-RC formation. Since levels of Orc1p (wild-type Orc1p or Orc1R694Ep) and Orc3p on chromatin were not so affected by expression of Orc1R694Ep as that of MCM (Figures 6B and 6C), Orc1R694Ep seems to

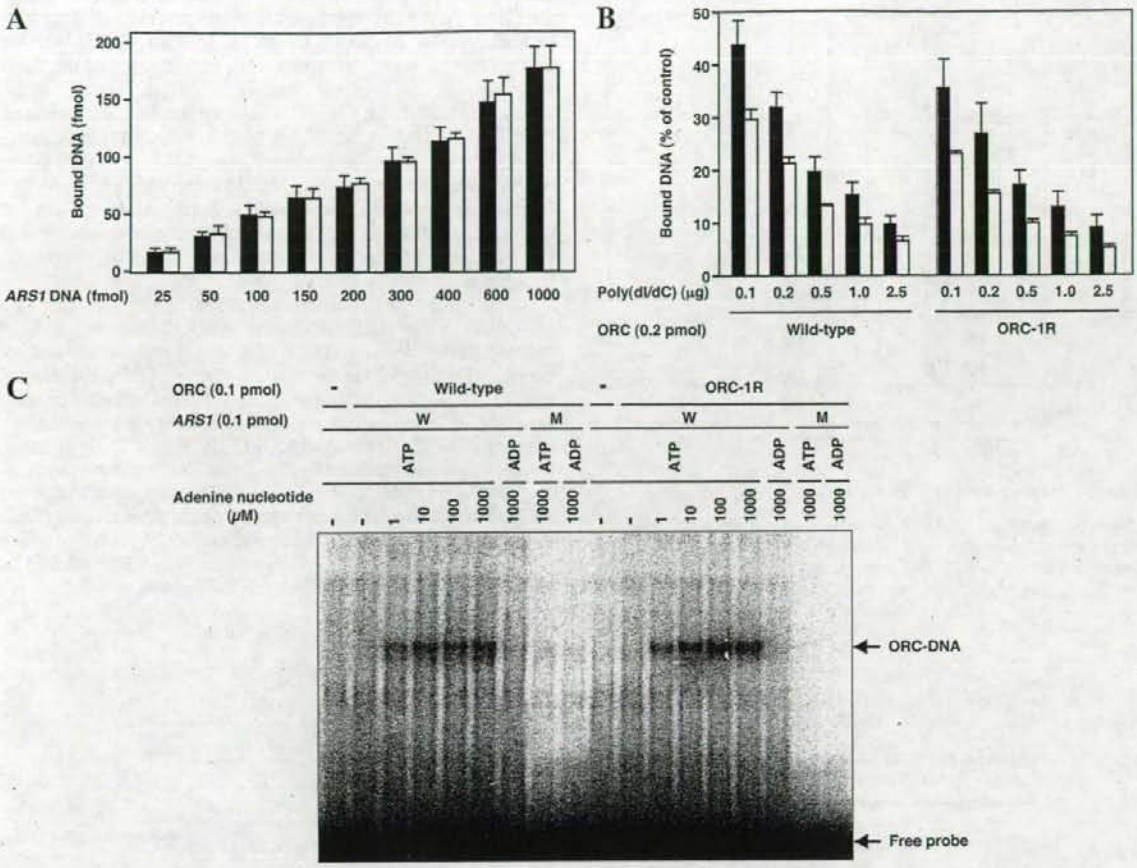

Figure 4 DNA-binding activity of ORC-1R

(**A**) Wild-type ORC (black bars) and ORC-1R (white bars) (0.2 pmol) were pre-incubated first with 5 mM ATP and then with radiolabelled *ARS1* DNA fragments, as indicated. DNA bound to ORC was determined by the filter-binding assay. Values are means ± S.D. ($n = 3$). (**B**) Wild-type ORC and ORC-1R (0.2 pmol) were pre-incubated first with 5 mM ATP, and then with poly(dI/dC) competitor as indicated, plus 0.4 pmol of radiolabelled DNA fragments [either wild-type *ARS1* (black bars) or mutant *ars1* (A$^-$B1$^-$; white bars)]. DNA bound to ORC was determined as described above. Without poly(dI/dC), wild-type ORC and ORC-1R bound 98.5 ± 19.6 and 109 ± 24.1 fmol of *ARS1* DNA respectively and 71.0 ± 19.0 or 84.3 ± 24.8 fmol of *ars1* DNA respectively. Values are means ± S.D. ($n = 3$). (**C**) Gel mobility-shift assay. Wild-type ORC and ORC-1R (0.1 pmol) were pre-incubated first with ATP or ADP, and then with 400 ng of poly(dI/dC) plus 0.1 pmol of radiolabeled DNA fragments [either *ARS1* (W) or *ars1* (M)] as described above. Samples were separated by PAGE and autoradiographed. Similar results were obtained in two independent experiments.

affect the functioning of ORC (pre-RC formation) rather than the presence of ORC on chromatin.

To confirm the results of chromatin-binding assay shown in Figures 6(B) and 6(C), we performed ChIP assay. As shown in Figure 6(D), both *ARS1* (origin) and *LEU2* (control) DNA fragments were approximately equally amplified when total DNA prepared from cells expressing wild-type Orc1p and Orc1R694Ep was used as the PCR template, indicating that the ChIP assay system has been established. Similar amplification was observed when immunoprecipitated DNA with an antibody specific for Orc3p was used as the template, confirming that ORC binding to origin DNA is not affected by overexpression of Orc1R694Ep (Figures 6D and 6E). On the other hand, overexpression of Orc1R694Ep resulted in less efficient amplification of *ARS1* DNA relative to *LEU2* DNA when immunoprecipitated DNA with an antibody specific for Myc (Mcm4p) was used as the template (Figures 6D and 6F), suggesting that overexpression of Orc1R694Ep inhibits preferential MCM binding to origin DNA – in other words, MCM loading on to origin DNA – and thus inhibited pre-RC formation.

We also examined the effect of overexpression of Orc1R694Ep on cell-cycle progression. To examine G1/S-phase transition and S-phase progression, cells were synchronized at G2/M phase. Orc1p or Orc1R694Ep was induced by incubation with galactose, and the cells then re-synchronized at G1 phase. Finally cells were released into fresh medium (Figure 6G). In this experiment, as a control, we used another mutant Orc1p (Orc1K485Tp), which has defective Walker A motif (we had previously shown that this mutant Orc1p does not function in yeast cells [22]). We confirmed that wild-type Orc1p, Orc1R694Ep and Orc1K485Tp are all approximately equally expressed on incubation with galactose (Figure 6H). As shown in Figure 6(I), G1/S-phase transition was similar in both strain yMT30 and strain yMT34 (DK186 cells expressing wild-type Orc1p and Orc1R694Ep respectively), but S-phase progression was slightly slower in strain yMT34. This is the first observation that mutant ORC with reduced ATPase activity can

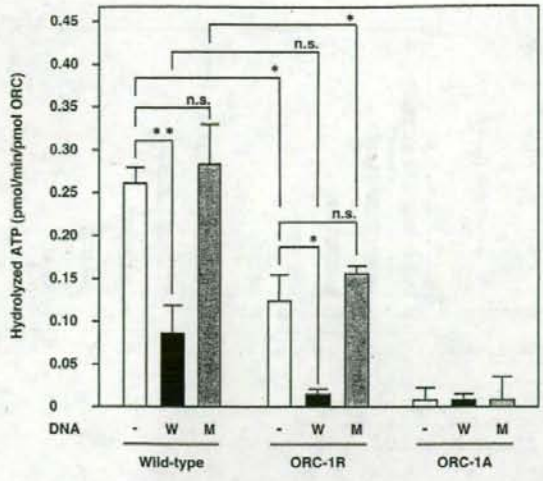

Figure 5 ATPase activity of ORC-1R

Wild-type ORC, ORC-1R and ORC-1A (0.3 pmol) were incubated with 10 μM radiolabelled ATP in the presence of 6 pmol of DNA fragments [either wild-type *ARS1* (W) or mutant *ars1* (M)]. ATPase activity is shown as ATP hydrolysed/min per pmol of ORC. Values are means $\pm$ S.D. ($n = 3$). $^{**}P < 0.01$; $^{*}P < 0.05$; n.s., not significant.

affect cell cycle progression. On the other hand, expression of Orc1K485Tp did not affect the cell-cycle progression. This may be because ORC containing Orc1K485Tp (ORC-1A) is inert for origin DNA binding – in other words, may not inhibit the wild-type ORC-binding to origin DNA – this being different from the case of ORC-1R. In other DNA-replication-related mutants, inefficient loading of MCM on to chromatin retards S phase [31,46]. Thus the slow S phase seen in Figure 6(I) may be due to the inefficient loading of MCM seen in Figures 6(B)–(F). Overall, the results in Figure 6 suggest that the ATPase activity of ORC stimulates MCM loading on to chromatin, and thus pre-RC formation, and is therefore important for the efficient progression of S phase.

As described in the Introduction, ORC with Orc1D569Yp or Orc1D569Fp, and ORC with Orc4R267Ap, also have reduced ATPase activity [27,28]. The Asp^{569} mutants showed reduced ATPase activity in the absence of origin DNA, but showed normal ATPase activity in its presence [27]. The Arg^{267} mutant showed no ATPase activity, either in the presence or in the absence of origin DNA [28], as seen with ORC-1A (Figure 5). By contrast, ORC-1R showed reduced ATPase activity in the absence of origin DNA, and double-stranded origin DNA fragments inhibited ATPase completely. The *in vitro* properties of these mutant ORCs differ, but all inhibited pre-RC formation (MCM loading), which strongly suggests that ORC ATPase stimulates MCM loading on to chromatin and thus stimulates pre-RC formation.

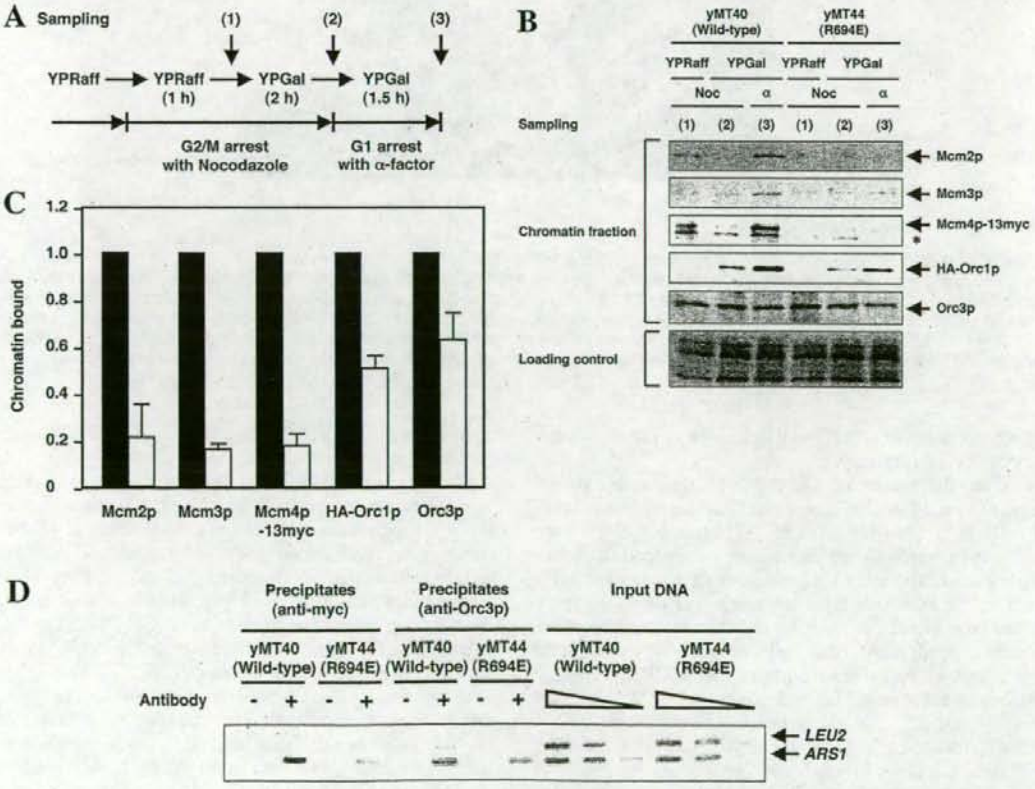

Figure 6 For legend see next page.

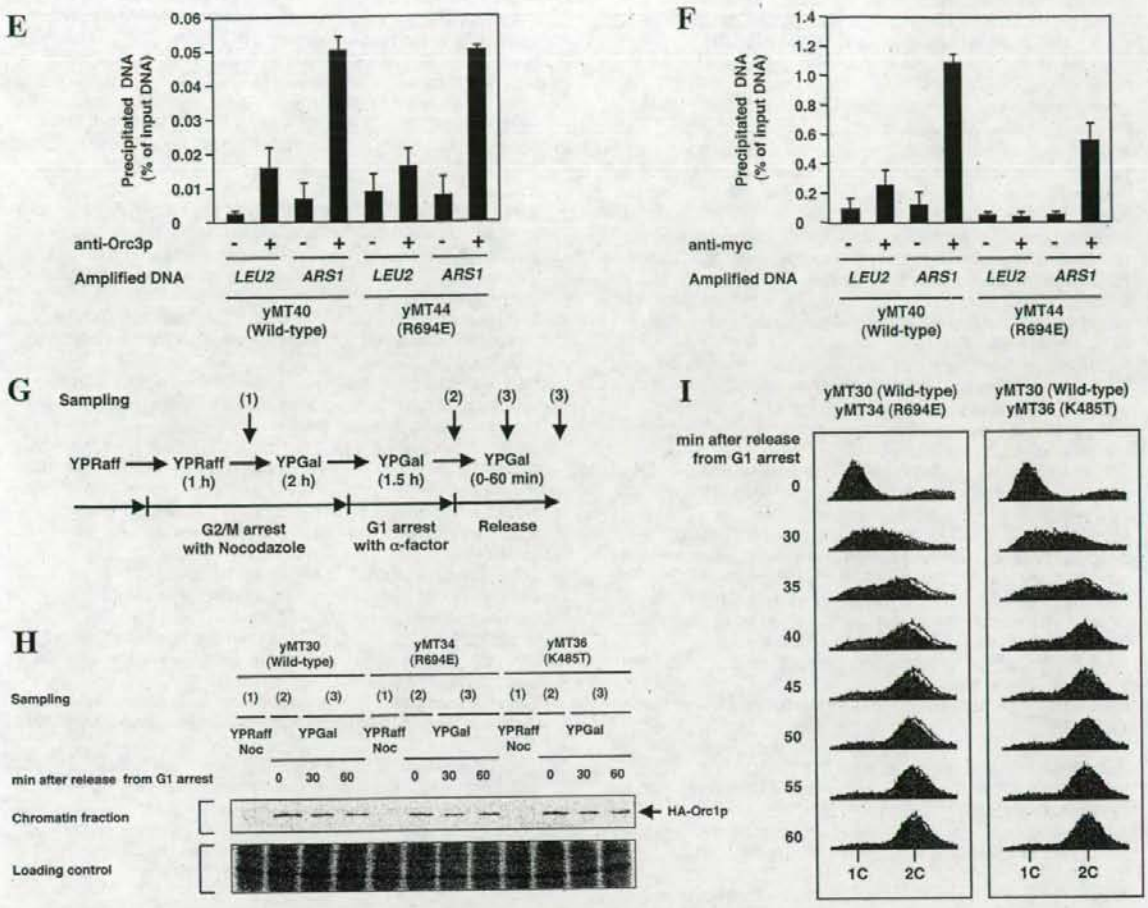

Figure 6 Effect of overexpression of Orc1R694Ep on pre-RC formation and cell-cycle progression

(**A**) Experimental outline and timing of sampling [(1), (2) and (3)]. Strain-yMT50 derivatives with expression plasmids for the wild-type HA-Orc1p or HA-Orc1R694Ep (yMT40 or yMT44 respectively) were cultured to exponential phase in YP medium with 2 % raffinose (YPRaff) and synchronized at G2/M phase by incubation with 10 μg/ml nocodazole (Noc) for 3 h [1 h in YPRaff, then 2 h in YPGal (YPRaff plus 2 % galactose)]. Then cells were washed and released into the fresh YPGal containing 0.1 μg/ml α-factor (α) and cultured for 1.5 h. (**B** and **C**) Chromatin fractions from the above were analysed by immunoblotting using monoclonal antibodies specific for Mcm2p, Mcm3p, Myc (for detection of Mcm4p–13Myc), HA (for detection of HA-Orc1p or HA-Orc1R694Ep) and Orc3p. As a loading control, the gel was stained with silver (**B**). Similar results were obtained in two independent experiments and the band intensity [at the sampling point (3)] was determined and expressed as mean $\pm$ S.D. ($n = 3$) (black bars, strain yMT44; white bars, strain yMT40). The amounts of each protein in strain yMT40 (black bars) were designated as 1, and those in yMT44 (white bars) are calculated relative to those in yMT40 (**C**). (**D**–**F**) Whole-cell extracts were immunoprecipitated with or without an antibody specific for Orc3p or Myc (for Mcm4p). DNA fractions were prepared from the immunoprecipitated samples ('Precipitates') and whole-cell extracts ('Input DNA') and subjected to PCR with specific primer sets for *LEU2* and *ARS1*. Titration of input DNA was shown by the gradient symbols in (**D**). The PCR products were separated in 3 % (w/v) agarose gel and visualized under UV light (**D**). Similar results were obtained in two independent experiments. (**E** and **F**) Band intensities were determined and expressed as means $\pm$ S.D. ($n = 3$). (**G**) Experimental outline. DK186 derivatives with expression plasmids for the wild-type HA-Orc1p, HA-Orc1R694Ep or HA-Orc1K485Tp (yMT30, yMT34 or yMT36 respectively) were synchronized in G2/M phase, induced with galactose and re-synchronized in G1 phase as described above. Finally, cells were washed and released into the fresh YPGal medium and sampled as indicated. (**H**) Chromatin fractions obtained as dscribed above were analysed by immunoblotting using monoclonal antibodies specific for HA (for detection of HA-Orc1p, HA-Orc1R694Ep or HA-Orc1K485Tp). As a loading control, the gel was stained with silver. Similar results were obtained in two independent experiments. (**I**) Cellular DNA contents were stained with propidium iodide and analysed by FACS. Black curve, strain yMT30; shaded area, strain yMT34 or yMT36. Similar results were obtained in two independent experiments.

We thank Professor Stephen P. Bell for baculovirus and plasmids, and Dr Bruce Stillman for antibodies. We also thank Dr Katsuhiko Shirahige, Dr Yuji Hori and Dr Douglas R. Kellogg for yeast strains. This work was supported by Grants-in-Aid for Scientific Research from the Ministry of Education, Culture, Sports, Science and Technology, Japan, the Asahi Glass Foundation, the Naito Foundation and the Kato Memorial Foundation.

REFERENCES

1 Sekimizu, K., Bramhill, D. and Kornberg, A. (1987) ATP activates dnaA protein in initiating replication of plasmids bearing the origin of the *E. coli* chromosome. Cell **50**, 259–265

2 Mizushima, T., Sasaki, S., Ohishi, H., Kobayashi, M., Katayama, T., Miki, T., Maeda, M. and Sekimizu, K. (1996) Molecular design of inhibitors of *in vitro* oriC DNA replication based on the potential to block the ATP binding of DnaA protein. J. Biol. Chem. **271**, 25178–25183

3 Mizushima, T., Takaki, T., Kubota, T., Tsuchiya, T., Miki, T., Katayama, T. and Sekimizu, K. (1998) Site-directed mutational analysis for the ATP binding of DnaA protein. Functions of two conserved amino acids (Lys-178 and Asp-235) located in the ATP-binding domain of DnaA protein *in vitro* and *in vivo*. J. Biol. Chem. **273**, 20847–20851

4 Katayama, T., Kubota, T., Kurokawa, K., Crooke, E. and Sekimizu, K. (1998) The initiator function of DnaA protein is negatively regulated by the sliding clamp of the *E. coli* chromosomal replicase. Cell **94**, 61–71

5 Mizushima, T., Nishida, S., Kurokawa, K., Katayama, T., Miki, T. and Sekimizu, K. (1997) Negative control of DNA replication by hydrolysis of ATP bound to DnaA protein, the initiator of chromosomal DNA replication in *Escherichia coli*. EMBO J. **16**, 3724–3730

6 Kurokawa, K., Nishida, S., Emoto, A., Sekimizu, K. and Katayama, T. (1999) Replication cycle-coordinated change of the adenine nucleotide-bound forms of DnaA protein in *Escherichia coli*. EMBO J. **18**, 6642–6652

7 Nishida, S., Fujimitsu, K., Sekimizu, K., Ohmura, T., Ueda, T. and Katayama, T. (2002) A nucleotide switch in the *Escherichia coli* DnaA protein initiates chromosomal replication: evidence from a mutant DnaA protein defective in regulatory ATP hydrolysis *in vitro* and *in vivo*. J. Biol. Chem. **277**, 14986–14995

8 Makise, M., Mima, S., Tsuchiya, T. and Mizushima, T. (2001) Molecular mechanism for functional interaction between DnaA protein and acidic phospholipids: identification of important amino acids. J. Biol. Chem. **276**, 7450–7456

9 Makise, M., Mima, S., Tsuchiya, T. and Mizushima, T. (2000) Identification of amino acids involved in the functional interaction between DnaA protein and acidic phospholipids. J. Biol. Chem. **275**, 4513–4518

10 Hase, M., Yoshimi, T., Ishikawa, Y., Ohba, A., Guo, L., Mima, S., Makise, M., Yamaguchi, Y., Tsuchiya, T. and Mizushima, T. (1998) Site-directed mutational analysis for the membrane binding of DnaA protein. Identification of amino acids involved in the functional interaction between DnaA protein and acidic phospholipids. J. Biol. Chem. **273**, 28651–28656

11 Sekimizu, K. and Kornberg, A. (1988) Cardiolipin activation of dnaA protein, the initiation protein of replication in *Escherichia coli*. J. Biol. Chem. **263**, 7131–7135

12 Makise, M., Mima, S., Katsu, T., Tsuchiya, T. and Mizushima, T. (2002) Acidic phospholipids inhibit the DNA-binding activity of DnaA protein, the initiator of chromosomal DNA replication in *Escherichia coli*. Mol. Microbiol. **46**, 245–256

13 Stillman, B. (1996) Cell cycle control of DNA replication. Science **274**, 1659–1664

14 Diffley, J. F. (1996) Once and only once upon a time: specifying and regulating origins of DNA replication in eukaryotic cells. Genes Dev. **10**, 2819–2830

15 Bell, S. P. (1995) Eukaryotic replicators and associated protein complexes. Curr. Opin. Genet. Dev. **5**, 162–167

16 Bell, S. P. and Dutta, A. (2002) DNA replication in eukaryotic cells. Annu. Rev. Biochem. **71**, 333–374

17 Bell, S. P. and Stillman, B. (1992) ATP-dependent recognition of eukaryotic origins of DNA replication by a multiprotein complex. Nature **357**, 128–134

18 Dutta, A. and Bell, S. P. (1997) Initiation of DNA replication in eukaryotic cells. Annu. Rev. Cell. Dev. Biol. **13**, 293–332

19 Klemm, R. D., Austin, R. J. and Bell, S. P. (1997) Coordinate binding of ATP and origin DNA regulates the ATPase activity of the origin recognition complex. Cell **88**, 493–502

20 Takenaka, H., Makise, M., Kuwae, W., Takahashi, N., Tsuchiya, T. and Mizushima, T. (2004) ADP-binding to origin recognition complex of *Saccharomyces cerevisiae*. J. Mol. Biol. **340**, 29–37

21 Makise, M., Takenaka, H., Kuwae, W., Takahashi, N., Tsuchiya, T. and Mizushima, T. (2003) Kinetics of ATP binding to the origin recognition complex of *Saccharomyces cerevisiae*. J. Biol. Chem. **278**, 46440–46445

22 Takahashi, N., Yamaguchi, Y., Yamairi, F., Makise, M., Takenaka, H., Tsuchiya, T. and Mizushima, T. (2004) Analysis on origin recognition complex containing Orc5p with defective Walker A motif. J. Biol. Chem. **279**, 8469–8477

23 Makise, M., Takahashi, N., Matsuda, K., Yamairi, F., Suzuki, K., Tsuchiya, T. and Mizushima, T. (2007) Mechanism for the degradation of origin recognition complex containing Orc5p with a defective Walker A motif and its suppression by overproduction of Orc4p in yeast cells. Biochem. J. **402**, 397–403

24 Lee, J. R., Makise, M., Takenaka, H., Takahashi, N., Yamaguchi, Y., Tsuchiya, T. and Mizushima, T. (2002) Inhibitory effects of acidic phospholipids on the binding of origin-recognition complex to origin DNA. Biochem. J. **362**, 395–399

25 Lee, J. R., Takenaka, H., Takahashi, N., Makise, M., Yamaguchi, Y., Tsuchiya, T. and Mizushima, T. (2002) Acidic phospholipids with unsaturated fatty acids inhibit the binding of origin recognition complex to origin DNA. J. Biochem (Tokyo). **131**, 541–546

26 Mendez, J. and Stillman, B. (2003) Perpetuating the double helix: molecular machines at eukaryotic DNA replication origins. Bioessays **25**, 1158–1167

27 Klemm, R. D. and Bell, S. P. (2001) ATP bound to the origin recognition complex is important for preRC formation. Proc. Natl. Acad. Sci. U.S.A. **98**, 8361–8367

28 Bowers, J. L., Randell, J. C., Chen, S. and Bell, S. P. (2004) ATP hydrolysis by ORC catalyzes reiterative mcm2-7 assembly at a defined origin of replication. Mol. Cell. **16**, 967–978

29 Speck, C., Chen, Z., Li, H. and Stillman, B. (2005) ATPase-dependent cooperative binding of ORC and Cdc6 to origin DNA. Nat. Struct. Mol. Biol. **12**, 965–971

30 Neuwald, A. F., Aravind, L., Spouge, J. L. and Koonin, E. V. (1999) AAA+: a class of chaperone-like ATPases associated with the assembly, operation, and disassembly of protein complexes. Genome Res. **9**, 27–43

31 Takahashi, N., Tsutsumi, S., Tsuchiya, T., Stillman, B. and Mizushima, T. (2002) Functions of sensor 1 and sensor 2 regions of *Saccharomyces cerevisiae* Cdc6p *in vivo* and *in vitro*. J. Biol. Chem. **277**, 16033–16040

32 Ogura, T., Whiteheart, S. W. and Wilkinson, A. J. (2004) Conserved arginine residues implicated in ATP hydrolysis, nucleotide-sensing, and inter-subunit interactions in AAA and AAA+ ATPases. J. Struct. Biol. **146**, 106–112

33 Bochtler, M., Hartmann, C., Song, H. K., Bourenkov, G. P., Bartunik, H. D. and Huber, R. (2000) The structures of HslU and the ATP-dependent protease HslU-HslV. Nature **403**, 800–805

34 Mizushima, T., Takahashi, N. and Stillman, B. (2000) Cdc6p modulates the structure and DNA binding activity of the origin recognition complex *in vitro*. Genes Dev. **14**, 1631–1641

35 Hori, Y., Shirahige, K., Obuse, C., Tsurimoto, T. and Yoshikawa, H. (1996) Characterization of a novel CDC gene (ORC1) partly homologous to CDC6 of *Saccharomyces cerevisiae*. Mol. Biol. Cell **7**, 409–418

36 Harvey, S. L. and Kellogg, D. R. (2003) Conservation of mechanisms controlling entry into mitosis: budding yeast wee1 delays entry into mitosis and is required for cell size control. Curr. Biol. **13**, 264–275

37 Sikorski, R. S. and Hieter, P. (1989) A system of shuttle vectors and yeast host strains designed for efficient manipulation of DNA in *Saccharomyces cerevisiae*. Genetics **122**, 19–27

38 Gietz, R. D. and Sugino, A. (1988) New yeast–*Escherichia coli* shuttle vectors constructed with *in vitro* mutagenized yeast genes lacking six-base pair restriction sites. Gene **74**, 527–534

39 Longtine, M. S., McKenzie, A., 3rd, Demarini, D. J., Shah, N. G., Wach, A., Brachat, A., Philippsen, P. and Pringle, J. R. (1998) Additional modules for versatile and economical PCR-based gene deletion and modification in *Saccharomyces cerevisiae*. Yeast **14**, 953–961

40 Reference deleted

41 Liang, C. and Stillman, B. (1997) Persistent initiation of DNA replication and chromatin-bound MCM proteins during the cell cycle in cdc6 mutants. Genes Dev. **11**, 3375–3386

42 Aparicio, O. M., Weinstein, D. M. and Bell, S. P. (1997) Components and dynamics of DNA replication complexes in *S. cerevisiae*: redistribution of MCM proteins and Cdc45p during S phase. Cell **91**, 59–69

43 Hingorani, M. M. and O'Donnell, M. (1998) ATP binding to the *Escherichia coli* clamp loader powers opening of the ring-shaped clamp of DNA polymerase III holoenzyme. J. Biol. Chem. **273**, 24550–24563

44 Marahrens, Y. and Stillman, B. (1992) A yeast chromosomal origin of DNA replication defined by multiple functional elements. Science **255**, 817–823

45 Rao, H. and Stillman, B. (1995) The origin recognition complex interacts with a bipartite DNA binding site within yeast replicators. Proc. Natl. Acad. Sci. U.S.A. **92**, 2224–2228

46 Schepers, A. and Diffley, J. F. (2001) Mutational analysis of conserved sequence motifs in the budding yeast Cdc6 protein. J. Mol. Biol. **308**, 597–608

Received 10 April 2007/1 April 2008; accepted 7 April 2008
Published as BJ Immediate Publication 7 April 2008, doi:10.1042/BJ20070484

Pharmaceutical Research, Vol. 25, No. 7, July 2008 (© 2008)
DOI: 10.1007/s11095-008-9549-8

Research Paper

Prolonging the *In Vivo* Residence Time of Prostaglandin E_1 with Biodegradable Nanoparticles

Tsutomu Ishihara,[1,4] Miyuki Takahashi,[1] Megumu Higaki,[1] Mitsuko Takenaga,[2] Tohru Mizushima,[3] and Yutaka Mizushima[1]

Received December 14, 2007; accepted January 29, 2008; published online February 22, 2008

Purpose. Prostaglandins have potent and diverse biologic activities, but their clinical application is severely restricted, mainly due to rapid inactivation *in vivo*. In order to modulate the pharmacokinetics of prostaglandin E_1 (PGE_1), we prepared biodegradable nanoparticles as a drug carrier.
Methods. Nanoparticles encapsulating PGE_1 were prepared from a blend of poly(lactic acid) homopolymer and poly(ethylene glycol)-poly(lactide) block copolymer by the solvent diffusion method in the presence of iron.
Results. PGE_1 was efficiently and stably embedded in the nanoparticles through interaction with iron, despite being relatively hydrophilic and having unstable chemical properties. Depending on the isomers and molecular weight of poly(lactic acid) selected, PGE_1 was gradually released from the nanoparticles at various rates into diluted serum *in vitro*. Both stable retention of PGE_1 in the nanoparticles and coating of the nanoparticles with poly(ethylene glycol) led to an extremely extended blood residence time of PGE_1, as well as preferential accumulation in vascular lesions.
Conclusions. These results suggest that the present strategy is useful to advance the clinical application of PGE_1 as a therapeutic agent for vascular disorders.

KEY WORDS: iron; nanoparticle; poly(lactic acid); prostaglandin E_1; vascular disorder.

INTRODUCTION

Prostaglandin E_1 is a member of the autocoid family that has diverse and potent biologic activities in many organ systems, such as vasodilation, angiogenesis, reduction of blood pressure, inhibition of platelet aggregation, cytoprotection, and suppression of cytokine production. The discovery of these activities has led to the application of PGE_1 as a therapeutic agent for use in the treatment of chronic arteriosclerosis obliterans, peripheral vascular disease, ulcers, hepatopathy, hypertension, diabetic neuropathy, and reperfusion injury (1,2). However, there have been two major obstacles to apply PGE_1 in clinical. One is rapid inactivation of PGE_1 during its first passage through the lungs (3), and another is severe side effects due to distribution to whole body. To overcome these obstacles, great efforts have been made to achieve the synthesis of chemically modified analogues that possess improved pharmacokinetics properties but share similar pharmacodynamic effects (4). Some analogues have been successfully developed, but their therapeutic application is still limited due to unanticipated side effects (5,6).

An alternative strategy consists of developing carriers for PGE_1, such as lipid emulsion (7–9), liposomes (10,11) and synthetic polymers (12,13), to modulate its pharmacokinetics. In 1983, one of the authors established a treatment technique using a lipid emulsion (so called lipid microspheres) with an average diameter of 0.2μm, which was composed of soybean oil, a drug and lecithin as the emulsifier (7). Lipid emulsion of PGE_1 (Lipo-PGE_1) is clinically used in Japan, South Korea, and China for systemic administration and shows a significantly superior clinical efficacy for peripheral vascular disease than PGE_1 clathrated in cyclodextrin (PGE_1CD: clinically used worldwide) because of its accumulation in damaged blood vessels (7,9,14). Despite enhancing the pharmacological activity of PGE_1, lipid emulsions and liposomes cannot retain PGE_1 stably under *in vivo* conditions due to their inherent structures and the relatively hydrophilic nature of PGE_1 (15,16).

On the other hand, polymeric solid particles seem to be promising carriers for the stable retention of drugs. Solid particles with a high retentiveness of PGE_1 would be expected to have the following advantages in terms of pharmacokinetics and pharmacodynamic. First, stable retention of PGE_1 by the solid particles would prevent its inactivation. Second, particles formed from biodegradable polymers such as poly(lactic/glycolic acid) (PLGA) and poly(lactic acid) (PLA), may allow PGE_1 to exhibit a long-term therapeutic effect by slow release along with degradation of the polymers (17). Third, the biodistribution of PGE_1 could be controlled by such particles

[1] DDS Institute, The Jikei University School of Medicine, 3-25-8 Nishi-shinbashi, Minato Tokyo 105-8461, Japan.
[2] Institute of Medical Science, St. Marianna University School of Medicine, 2-16-1 Sugao, Miyamae, Kawasaki Kanagawa 216-8512, Japan.
[3] Graduate School of Medical and Pharmaceutical Sciences, Kumamoto University, 5-1 Oe-honcho, Kumamoto 862-0973, Japan.
[4] To whom correspondence should be addressed. (e-mail: ishihara@jikei.ac.jp)

0724-8741/08/0700-1686/0

and specific delivery to target sites should enhance its therapeutic effects while reducing side effects. In general, colloid particles that are administered systemically undergo uptake by the mononuclear phagocyte system (MPS), resulting in accumulation in the liver and spleen. On the other hand, the pioneering work by Langer's group showed that polymeric nanoparticles (micelles) formed from poly(ethylene glycol)-block-poly(lactide) (PEG-PLA) copolymers could remain in the circulation for a prolonged period because the steric barrier of PEG chains on their surface reduced interaction with opsonins and cells of the MPS (18). Furthermore, these long-circulating nanoparticles show preferential accumulation in tumors and sites of inflammation due to the enhanced permeability and retention (EPR) effect (19,20). These nanoparticles may be an attractive carrier for delivery of PGE_1 to target sites such as vascular lesions.

In order to take advantage of these properties, it is necessary to establish a method for preparing nanoparticles with a high retentivity and high content of PGE_1. However, it is difficult to encapsulate hydrophilic drugs in solid particles although hydrophobic drugs can easily be encapsulated by hydrophobic interactions (21). Some methods (e.g. the water-in-oil-in-water solvent evaporation method) achieve the efficient encapsulation of hydrophilic drugs in larger solid particles (microparticles), but these methods generally cannot produce small nanoparticles for systemic administration (22,23). We previously reported that PLGA/PLA nanoparticles (less than 200nm in diameter) encapsulating water-soluble betamethasone phosphate with a high efficiency could be successfully prepared by an oil-in-water solvent diffusion method in the presence of zinc (24,25). We found that zinc increased the encapsulation efficiency of betamethasone phosphate in the nanoparticles by formation of a water-insoluble complex with the betamethasone phosphate (24). It was considered that this strategy of using a metal ion might also be suitable for incorporation and retention of PGE_1 in PLGA/PLA nanoparticles.

In the present study, we prepared PGE_1-encapsulated nanoparticles formed from a mixture of PEG-PLA block copolymers and PLA, and evaluated the retention of PGE_1, its release profile, and the accumulation in vascular lesions.

MATERIALS AND METHODS

Materials

Poly (D, L-lactic acid) (PDLLA) and poly (L-lactic acid) (PLLA) were supplied by Taki Chemical Co., Ltd. (Hyogo, Japan). The molecular weight of the polymers was determined by gel permeation chromatography and the composition is shown as *PDLLA (Mw kDa)* or *PLLA (Mw kDa)*. Poly(ethylene glycol)-poly (D, L-lactide) (PEG-PDLLA) block copolymer was synthesized by ring-opening polymerization of D, L-lactide (Purac America, IL, USA) in the presence of monomethoxy-PEG (Mw 5200; NOF Co., Tokyo, Japan) according to the reported method (26,27). The composition and molecular weight of the block copolymers were evaluated by ^{1}H-NMR and gel permeation chromatography. PEG-PDLLA with an average Mw 14,900 was used in this study. Prostaglandin E_1 (PGE_1) was purchased from Cayman Chemical Co. and PGE_1 clathrated in cyclodextrin (PGE_1CD) was purchased from Ono Pharmaceutical Co. Ltd. (Osaka, Japan). Cy7-COOH monomer was obtained by alkali hydrolysis of Cy7-NHS ester (GE Healthcare) and subsequent HPLC purification.

Solubility of PGE_1

Crystalline PGE_1 was dissolved in ethanol at various concentrations and then the solution was added to a ninefold volume of water, 10 mM HCl aqueous solution, or phosphate-buffered saline (PBS, pH7.2). After incubation for 30 min at 25°C, the resulting solution was centrifuged at 16,000×*g* for 10 min *to precipitate insoluble PGE_1*. The residual PGE_1 in the supernatant was determined by HPLC with a Nova Pak-C18 column (Waters) and a UV-Vis detector (absorbance at 193 nm), using water (pH adjusted to 3.5 with acetic acid)/acetonitrile (*v/v* = 79:21) as the mobile phase.

To a freshly prepared aqueous solution of iron (III) chloride ($FeCl_3$) hexahydrate, various amounts of diethanolamine (DEA) were added rapidly. Next, an ethanol solution of PGE1 was added to a ninefold excess volume of the resulting solution or suspension. The final concentrations of PGE_1 and $FeCl_3$ were fixed at 0.56 and 10 mM, respectively. After incubation for 30 min at 25°C, the pH of the solutions/suspensions was monitored and then centrifugation was done at 16,000×*g* for 10 min *to precipitate insoluble PGE_1*. The supernatant (100 µl) was mixed with 400 µl of an aqueous citrate solution (10 mM, pH7.2), and the PGE_1 content was determined by HPLC as mentioned above.

Preparation of Nanoparticles

Nanoparticles were prepared by the oil-in-water solvent diffusion method in the presence of iron. Block copolymers, 5 mg of PGE_1, and diethanolamine (DEA) were dissolved in 525µl of acetone, while PLLA was dissolved in 225 µl of 1,4-dioxane at 50°C. The total amount of block copolymers and homopolymer was fixed at 25 mg and the blending ratio of these polymers influenced the PEG content. After mixing these solutions, iron (III) chloride anhydrous acetone solution (500 mM) was added. The resulting mixture was allowed to stand for 10 min at room temperature. To 25 ml of distilled water stirred at 1,000 rpm, the mixture was added dropwise at the rate of 48 ml/h using a 26G needle. During diffusion of the organic solvent into water, nanoparticles formed rapidly along with the solidification of PLA and the block copolymers. Immediately, 2.5 ml of aqueous 0.5M citrate solution (pH7.2) and 125 µl of aqueous 200 mg/ml Tween 80 solution were added to the resulting nanoparticle suspension to chelate iron (III) and enhance stable dispersion of the nanoparticles, respectively. Finally, the nanoparticles were purified and concentrated by ultrafiltration (Centriprep YM-50, Amicon).

Nanoparticles encapsulating dyes (rhodamine or Cy7) were prepared similarly by adding a small amount of either PLA-dye conjugate. The conjugates were synthesized by coupling the dyes with an amino group introduced into the PLA chain. One milliliter of an aqueous solution of ethylenediamine dihydrochloride (530 mg/ml) was mixed with 27 ml of DMSO containing *PDLLA(18)* (1,000 mg), 1-ethyl-3-(3-dimethylaminopropyl) carbodiimide hydrochloride (380mg), *N*-hydroxysuccinimide

(230 mg), and 4-(dimethylamino)-pyridine (270 mg), and the resulting solution was allowed to stand for 1day at room temperature. The synthesized PLA-ethylenediamine conjugate was purified by precipitation in an excess volume of water. PLA-dye conjugates were synthesized by mixing the PLA-ethylenediamine conjugate with rhodamine isothiocyanate or Cy7-NHS ester in DMSO and were purified by precipitation in an excess volume of isopropanol. The conjugates were characterized by gel permeation chromatography using TSKgel α-4000, α-3,000, and α-2500 columns (TOSOH Co., Tokyo, Japan), with DMF containing 10 mM $LiCl_2$ as the mobile phase. The amount of dye in the conjugates was determined by UV-Vis spectrometry. The conjugates used in this study contained 7.2nmol of rhodamine and 13.5nmol of Cy7 in 1 mg, respectively. Nanoparticles containing rhodamine were also formed from PLLA in the absence of block copolymers by the addition of 4.5 ml of acetone solution containing 25 mg of *PLLA (20)*, 1 mg of *PDLLA(18)*-rhodamine conjugate, 45 μmol of DEA, 5 mg of PGE_1, and 7.5μmol of iron (III) chloride to 25 ml of a 0.5% aqueous solution of Tween 80.

A lipid emulsion incorporating PGE_1 (Lipo-PGE_1) was prepared according to the published method (9). Lipo-PGE_1 with Cy7 was also prepared similarly by mixing with a small amount of Cy7-(dipalmitoyl-phosphatidylethanol amine) conjugate. The conjugate was synthesized by mixing Cy7-NHS ester, dipalmitoyl-phosphatidylethanol amine, and dimethylamino pyridine in chloroform/methanol (1/1 = *v/v*), and was purified by HPLC.

Characterization of Nanoparticles

The particle size and distribution were determined by the dynamic light scattering method (FPAR-1000, Otsuka Electronics, Ltd., Osaka, Japan), and the weighted average diameter was calculated by Marquadt's method.

The PGE_1 content of the nanoparticles was determined as follows. The nanoparticle suspension (50 μl) was evaporated in a vacuum centrifugal concentrator at 50°C. The dried nanoparticles were dissolved in 150 μl of 1,4-dioxane. Next, 150 μl of acetonitrile containing 9 μg of 3-phenylpropionate as an internal standard and 1,700 μl of an aqueous EDTA solution (50 mM, pH3.5) were added in this order. After 20 min, the solution was applied to a C18 reverse phase cartridge column (SepPak C18 200 mg, Waters). After washing the column with 6 ml of water, PGE_1 was eluted with 3 ml of acetonitrile, and the eluate was mixed with an equal volume of 9-anthryldiazomethane (ADAM: Funakoshi Co. Ltd.; Tokyo, Japan) in acetonitrile (0.2 mg/ml). After incubation of this mixture for 18h at 37°C, the PGE_1 content was determined by HPLC with a ZORBAX Eclipse XDB-C8 column (Agilent) and a fluorescence detector (excitation at 365 nm/emission at 412 nm).

The encapsulation efficiency of PGE_1 in the nanoparticles was defined as the ratio of the weight of PGE_1 to the total weight of PLA in the nanoparticles. Total PLA was calculated from the amount of lactic acid produced by the degradation of PLA and PEG-PLA (28). The purified nanoparticle suspension was mixed with an equal volume of 4N NaOH in water and the mixture was incubated for 18h at 50°C. After the addition of a ninefold excess of 340 mM phosphoric acid in water, the lactic acid content of the solution was determined by HPLC using an Inertsil ODS-2 column (GL Sciences Inc.) with detection at 220 nm.

Profile of PGE_1 Release from Nanoparticles

PGE_1-encapsulated nanoparticles prepared from various polymers were dispersed in a mixture of fetal bovine serum (FBS) and phosphate-buffered saline (PBS) (50% *v/v*, pH7.2) at a PGE_1 concentration of 100 μg/ml. After incubation at 37°C for the specified times, each suspension (100 μl) was diluted with 900 μl of 50 mM EDTA solution (pH7.0) and was centrifuged at 40,000×*g* for 30 min. After washing the precipitate with 1 ml of distilled water by centrifugation, the PGE_1 content was determined by HPLC as described above.

Interaction Between Nanoparticles and Cells

RAW 264.7 cells (a murine macrophage-like cell line) were added to an eight-well chamber plate at 1×10^5 cells per well and incubated overnight at 37°C in MEM containing 10% FBS. The cells were washed with PBS and incubated in 300 μl of fresh medium with rhodamine-encapsulated nanoparticles for 2h at 37°C. Next, the cells were washed six times with PBS and were fixed with 4% paraformaldehyde solution. After nuclear staining with diamino-phenylindole (DAPI), the cells were observed under a fluorescence microscope (IX71; Olympus Co., Tokyo, Japan).

Animal Experiments

Male Wistar rats (7weeks old, weighing 210–230 g) were obtained from SLC (Shizuoka, Japan) and were used to determine the blood concentration profile of PGE_1. The formulations of PGE_1 (nanoparticles, lipo-PGE_1, and PGE_1CD) were administered intravenously via the tail vein at a PGE_1 dose of 133 μg/kg. At designated intervals, blood was collected from the retro-orbital plexus, and then 50μl of blood was mixed with 400μl of 1,4-dioxane and subsequently with 50μl of 10 mM EDTA aqueous solution (pH7). Because PGE_1 and PLA are soluble in 1,4-dioxane, an excess of 1,4-dioxane was used to extract PGE_1 from the nanoparticles in addition to precipitating serum proteins. The mixture was agitated thoroughly and was centrifuged at 12,000rpm for 10 min. The supernatant (200 μl) was dried in a vacuum centrifugal concentrator at 50°C and then was redissolved in 50 mM Tris–HCl buffer (pH7.5) containing 9 mg/ml NaCl, 1.5 mg/ml bovine serum albumin, 1 mM $MgCl_2$, and 0.5 mM $ZnCl_2$. The PGE_1 content was determined by using a PGE_1 enzyme immunoassay kit (R&D Systems Inc., Minnesota) according to the manufacturer's protocol. As a preliminary experiment, each PGE_1 formulation was added to blood collected from a rat without any treatment and the PGE_1 content of the blood was determined by the method mentioned above. In each case, PGE_1 could be detected effectively and the values corresponded with those determined by HPLC, indicating that all PGE_1 in the blood was detectable independent of the formulation.

The accumulation of nanoparticles in vascular lesions was evaluated by *in vivo* fluorescence imaging. A rat model of peripheral vascular disease was created according to the reported method (29,30). In brief, male Wistar rats weighing

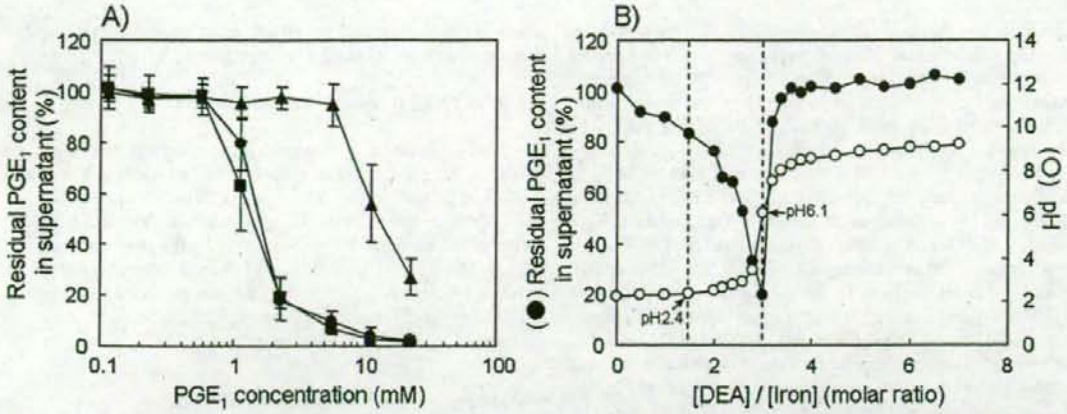

Fig. 1. Solubility of prostaglandin E_1 (PGE_1) in aqueous solutions. **A** An ethanol solution of PGE_1 with various concentrations was added to a ninefold excess volume of water (*circle*), 10 mM HCl aqueous solution (*square*), or PBS (pH 7.2) (*triangle*). After centrifugation, the residual PGE_1 in the supernatant was determined by HPLC. Each data point represents the mean±SD of three independent experiments. **B** An ethanol solution of PGE_1 was added to a ninefold excess volume of various iron (III) chloride solutions with different pH levels. The pH was adjusted by addition of diethanolamine (DEA). The final concentrations of PGE_1 and iron (III) chloride were fixed at 0.56 and 10 mM, respectively. After centrifugation, the residual PGE_1 in the supernatant was determined by HPLC.

260–280 g were anesthetized with pentobarbital (50 mg/kg, i. p.). The right femoral artery was exposed by incision and 150μl of a sodium laurate solution (5 mg/ml in 5% glucose) was injected. Next, hemostasis was achieved and the incision was sutured. After 1day, 700μl of saline containing Cy7-loaded nanoparticles, Cy7-loaded lipo-PGE_1 or Cy7-COOH monomer (each Cy7 concentration = 1.2μM) was intravenously administered via the tail vein. One day after administration, fluorescence images of the right hind paw were obtained with an *in vivo* fluorescence imaging system (eXplore Optix micro optical imager, GE Healthcare). The photon counts of the images were normalized by using the attached software. All animal experiments were performed in accordance with the Animal Experiment Guidelines of the Jikei University School of Medicine.

RESULTS AND DISCUSSION

Crystalline PGE_1 is soluble in organic solvents such as ethanol, 1,4-dioxane, DMSO, and acetone, but is only sparingly soluble in aqueous solutions. Therefore, we examined the solubility of PGE_1 in various aqueous solutions

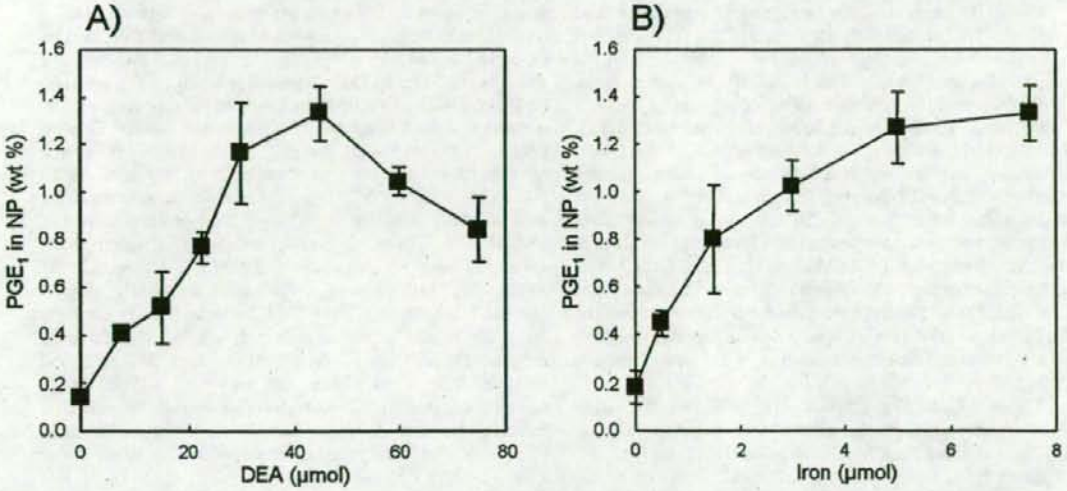

Fig. 2. Preparation of PGE_1-encapsulated nanoparticles from a blend of block copolymer and poly(lactic acid). **A** Effect of DEA on the encapsulation of PGE_1 in nanoparticles. Nanoparticles were prepared from a mixture of PEG-PDLLA and *PLLA(20)* with a 30% PEG content in the presence of 7.5 μmol iron. **B** Effect of iron and DEA on the encapsulation of PGE_1 in nanoparticles. Nanoparticles were prepared from a mixture of PEG-PDLLA and *PLLA(20)* with a 30% PEG content in the presence of DEA and iron (the molar ratio of DEA to iron was 6:1). Each data point represents the mean±SD of three independent experiments.

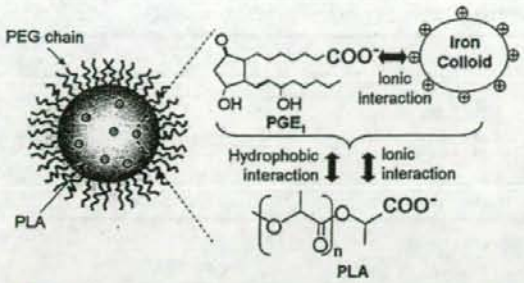

Fig. 3. Schematic illustration of nanoparticle encapsulating PGE_1.

containing 10% ethanol. The saturation limit of PGE_1 in water or a 10 mM aqueous solution of HCl was about 0.56 mM, while its solubility in PBS (pH7.2) was higher (5.6 mM) due to deprotonation of the carboxyl group (Fig. 1A). These findings indicated that PGE_1 would be soluble at a concentration of 0.56 mM in aqueous solutions, even if its carboxyl group is protonated. This level of solubility is relatively high compared with other drugs that are incorporated into solid particles (21). Although it would also depend on the method of preparation, this high solubility of PGE_1 could reduce its incorporation within solid particles. Thus, we tried to decrease the solubility of PGE_1 by formation of a complex with iron.

Iron is one of the essential minerals for life. Although iron chemistry is complicated, iron salts have been widely used in various clinical applications. The species of iron (III) chloride in aqueous solutions are conventionally classified into an unpolymerized fraction, a polymerized fraction (polymeric iron chloride produced by the hydrolysis of iron chloride), and a precipitated fraction (31,32). Although the factors that determine polymerization or subsequent precipitation are still not well understood, these processes seem to be influenced by variables such as the concentrations of iron and base, the type of base, the hydrolysis rate, mixing conditions, temperature and aging period (31,32). In an iron (III) chloride solution with a low pH, iron colloids consisting of polymeric iron chloride, iron hydroxide, or iron oxide hydroxide reach several nanometers in diameter and have a positively charged surface that can electrostatically interact with negatively charged molecules (31–33). On the other hand, at the isoelectric point (pH6–8.6), the surface charge of the colloids is neutralized and precipitates of iron colloids are preferentially formed (34). In agreement with such reports, our experiments showed the formation of colloids 5–15nm in diameter with positive zeta potentials at a low pH, while precipitates of the iron colloids formed at a high pH. Figure 1B shows the solubility of PGE_1 in 10 mM aqueous solutions of iron (III) chloride with different pH values adjusted by the addition of DEA. At a pH between 2.4 and 6.1, the residual PGE_1 content of the supernatant obtained after centrifugation of the solution gradually decreased along with the pH and the minimum content was seen at pH6.1. This indicated that electrostatic complexes were formed by PGE_1 and iron colloids along with deprotonation of the carboxyl group of PGE_1. On the other hand, at a pH lower than 2.4 and a pH higher than 6.1, most PGE_1 remained in the supernatant and did not form complexes, probably due to protonation of the carboxyl group of PGE_1 and neutralization of the positive charge of the iron colloids, respectively.

The formation of water-insoluble complexes of PGE_1 is expected to lead to its efficient incorporation into solid particles. In the present study, nanoparticles were prepared from PLA, PEG-PLA block copolymer, and PGE_1 by the solvent diffusion method in the presence of iron and DEA. In order to optimize the conditions for efficient encapsulation of PGE_1, various types of nanoparticles were prepared by altering the ratios of the additives. As shown in Fig. 1B, the amount of DEA added was crucial for formation of a water-insoluble complex of PGE_1. Therefore, the influence of the amounts of DEA and iron added on encapsulation of PGE_1 by the nanoparticles was examined. In the absence of both iron and DEA, PGE_1 was not incorporated into the nanoparticles (encapsulation efficiency was below 0.2wt%) due to its rapid diffusion out of the organic phase into the aqueous phase during the process of solidification of PLA and the block copolymer (formation of solid nanoparticles). On the other hand, in the presence of a constant amount of iron (7.5μmol), increasing the amount of DEA added led to a marked increase in the encapsulation of PGE_1 and the maximum incorporation occurred with 45μmol of DEA (Fig. 2A). In contrast, DEA could not enhance the incorporation of PGE_1 in the absence of iron. DEA probably acted to neutralize the acidic environment derived from iron chloride by its buffering effect, as shown in Fig. 1B, because similar results were also obtained when using other basic reagents (triethanolaimine and dimethylamino pyridine) instead of DEA (data not shown). These results indicated that both DEA and iron were essential for effective encapsulation of PGE_1. Furthermore, maximum incorporation of PGE_1 occurred with the addition of specific amount of DEA as well as the formation of complexes between PGE_1 and iron colloids (Fig. 1B), suggesting that PGE_1 was incorporated in the nanoparticles by the formation of complexes with iron colloids. However, maximum encapsulation of PGE_1 was

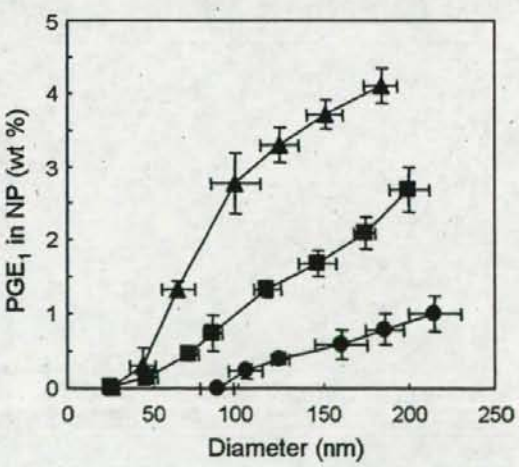

Fig. 4. Effect of the molecular weight of PLLA homopolymers on the encapsulation of PGE_1 in nanoparticles. Nanoparticles were prepared by altering the blending ratio of PEG-PDLLA and PLLA with various molecular weights [*triangle: PLLA(5), square: PLLA(20), circle: PLLA(33)*]. Each data point represents the mean±SD of three independent experiments.

Table I. Characteristics of Nanoparticles Formed From Various Blends of Block Copolymer and Poly(lactic acid)

Codes	PLA (Mw kDa)	Blend ratio (% of PEG content in the blend)	PGE_1 in nanoparticle (wt%)	Diameter (nm)	Polydispersity index
NP-L33	*PLLA(33)*	40	0.40±0.08	124±5	0.091
NP-L20	*PLLA(20)*	30	1.33±0.12	117±8	0.075
NP-L20s	*PLLA(20)*	45	0.47±0.06	71±5	0.051
NP-L5	*PLLA(5)*	15	3.30±0.23	124±11	0.104
NP-DL18	*PDLLA(18)*	20	1.22±0.11	121±7	0.088

*The mean (±SD) was calculated from three nanoparticle suspensions prepared independently.

observed at a DEA:iron molar ratio of 6:1, while the complex formed at a molar ratio of 3:1 (Fig. 1B). This may have occurred because excess DEA is necessary to neutralize the acidic environment induced by PLA with a terminal carboxyl group in the case of incorporating PGE_1 into nanoparticles. The encapsulation efficiency of PGE_1 also increased and almost reached a plateau along with an increase in the total amount of iron and DEA added at a constant molar ratio (DEA/iron = 6:1) (Fig. 2B). Taken together with the results shown in Fig. 2A, it was concluded that 7.5μmol of iron is adequate for efficient encapsulation of PGE_1at this scale of preparation.

Figure 3 shows the putative mechanism of PGE_1 encapsulation by nanoparticles. Deprotonated PGE_1 interacts ionically with positively charged iron colloids, at the specified pH obtained by adding DEA, resulting in the formation of a water-insoluble complex. The PGE_1 complex is efficiently incorporated by the nanoparticles through a hydrophobic interaction with PLA during the process of solidification of PLA and the block copolymers, while free PGE_1 is poorly incorporated due to its rapid diffusion into the aqueous phase (35). However, it is still unclear whether the complex formed in the organic solvent or during the process of diffusion from the organic solvent into the aqueous phase.

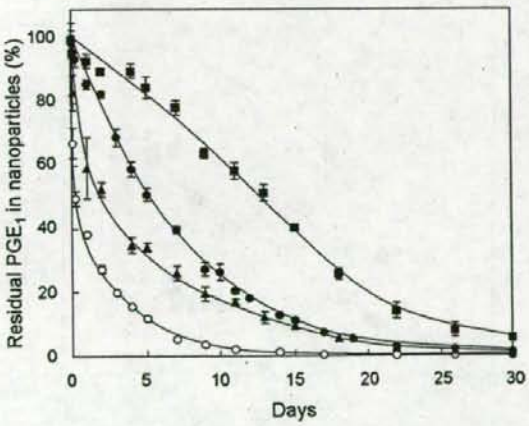

Fig. 5. Release profile of PGE_1 from nanoparticles suspended in FBS/PBS solution (50% *v/v*, pH 7.2) at 37°C. The different nanoparticles (*square: NP-L33, filled circle: NP-L20, triangle: NP-L5*, and *open circle: NP-DL18* listed in Table I) had almost the same diameter, but were formed from PLA with different compositions. Each data point represents the mean±SD of three independent experiments.

We also examined the effect of particle size and the molecular weight of PLA on encapsulation of PGE_1. Nanoparticles with various diameters were prepared by changing the blending ratio of block copolymers and PLA homopolymers with different molecular weights (Fig. 4). When block copolymers were mixed at a high ratio, there was a decrease in the diameter of the nanoparticles, indicating that the copolymers have a surfactant effect (36). The efficiency of encapsulating PGE_1 in the nanoparticles increased markedly along with particle size. This may have been because PGE_1 was more effectively retained by large particles during the process of solidification of PLA, since large particles have a smaller relative surface area compared with small particles. On the other hand, the efficiency of encapsulation increased as the molecular weight of PLA homopolymers decreased. This suggests that the PLA homopolymers acted as a reservoir of PGE_1 by ionic interaction between the residual positive charge on the PGE_1-iron colloid complex and the terminal carboxyl group of the PLA chain in addition to a hydrophobic interaction (Fig. 3), because it has been reported that cationic molecules (drugs) can be embedded in PLGA particles in a similar electrostatic manner (37).

We prepared various nanoparticles with different diameters and compositions (Table I), and then evaluated their characteristics *in vitro* and *in vivo*. In order to examine the influence of changes to the composition of PLA (such as isomers and molecular weights), four different kinds of nanoparticles (*NP-L33*, *-L20*, *-L5*, and *-DL18*) with approximately the same diameter were prepared. In addition, nanoparticles (*NP-L20 and -L20s*) with different diameters were prepared by altering the blend ratio of *PLLA(20)* and PEG-PDLLA. The release of drugs from biodegradable particles in buffered solutions is influenced by various factors such as particle diameter, composition, temperature, ionic strength, pH, and the presence of biological components. We evaluated the release of PGE_1 from nanoparticles dispersed in diluted serum (FBS/PBS 50% *v/v*, pH7.2) at 37°C (Fig. 5). It was found that the nanoparticles formed from *PDLLA(18)* (*NP-DL18*) released PGE_1 faster than those formed from *PLLA(20)* (*NP-L20*), while nanoparticles prepared from PLLA homopolymers with a lower molecular weight (*NP-L5*) tended to release PGE_1 faster than those prepared from homopolymers with a higher molecular weight (*NP-L33*), despite the similar size of these nanoparticles. Thus, nanoparticles prepared from PLLA instead of PDLLA or those prepared from PLLA with a higher molecular weight showed slower release of PGE_1. Racemic PDLLA and isotactic PLLA have different physicochemical properties (38). For example, PDLLA is an amorphous polymer, but PLLA is semi-crystalline. The glass-transition

temperature (*Tg*) of PLLA is higher than that of PDLLA, and hydrolysis of PLLA is slower. These properties also depend on the molecular weight of the polymers. Therefore, the release rate of PGE_1 might be regulated by complicated factors such as the thermodynamic stability, kinetic stability, and degradation rate of the nanoparticles. Because gradual release of PGE_1 from *NP-L33* and *NP-L20* occurred without an initial burst, this supported complete incorporation of PGE_1 into the nanoparticles rather than adsorption to the particle surface.

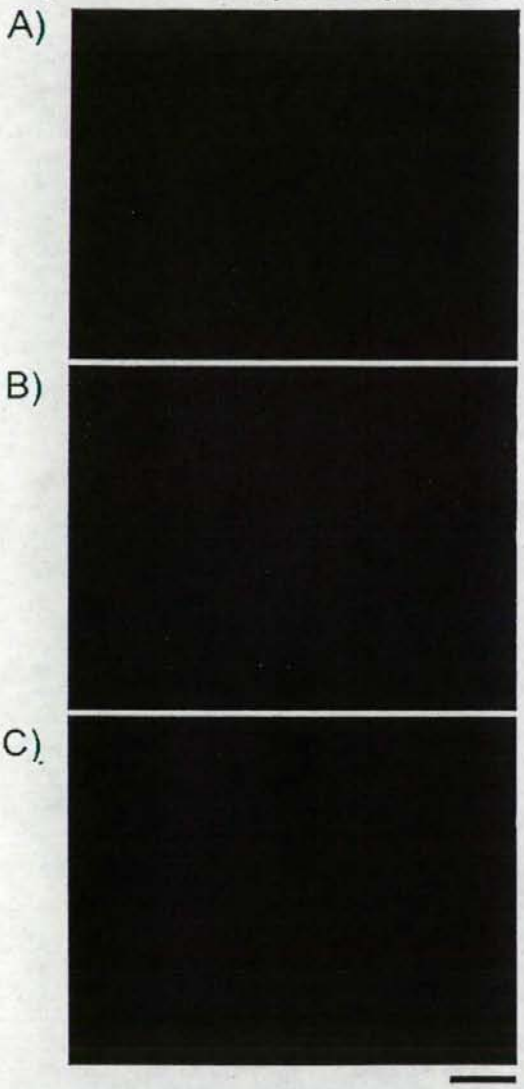

Fig. 6. Fluorescence images of RAW 264.7 cells after incubation with **A** rhodamine, **B** rhodamine-encapsulated nanoparticles prepared from *PLLA (20)* without PEG-PDLLA, and **C** rhodamine-encapsulated nanoparticles prepared with PEG-PDLLA (*NP-L20* in Table I). Blue and red images show nuclear staining by DAPI and rhodamine, respectively. Scale bar=50 μm.

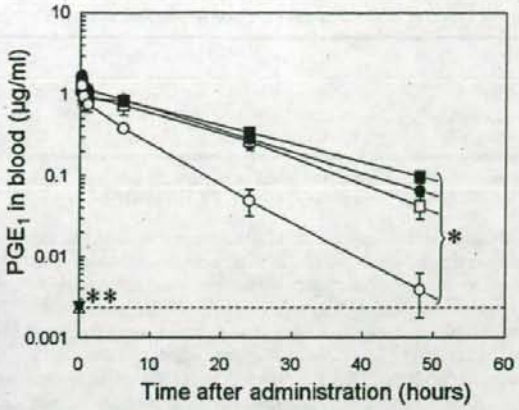

Fig. 7. Clearance of PGE_1 from the blood in rats. Various nanoparticles and other formulations incorporating PGE_1 (*triangle: Lipo-PGE_1, inverted triangle: PGE_1CD, filled circle: NP-L33, open square: NP-L20, filled square: NP-L20s, open circle: NP-DLI8* in Table I) were injected intravenously at a PGE_1 dose of 133 μg/kg. Among the nanoparticles, *NP-L33*, *NP-L20*, and *NP-DLI8* had approximately the same diameter, but were formed from PLA with different compositions. *NP-L20s* was formed from the same polymers as *NP-L20*, but was smaller than all the other nanoparticles. Each data point represents the mean±SD of three rats. Below the detection limit (0.0023 μg/ml) after 72 h (*asterisk*) or after 5 min (*double asterisk*).

Overall, it was demonstrated that it is possible to prepare nanoparticles with various PGE_1 release characteristics, depending on the isomers and molecular weight of the PLA homopolymers used.

Coating of particles with PEG has been reported to have a marked influence on their interaction with MPS cells both *in vitro* and *in vivo* (39). When the interaction of rhodamine-encapsulated nanoparticles with macrophage-like cells (RAW 264.7 cells) was observed by fluorescence microscopy (Fig. 6), nanoparticles made with PEG-PDLLA (*NP-L20*) showed significantly less internalization by cells (Fig. 6C) than nanoparticles which do not contain PEG (Fig. 6B), indicating sufficient masking by PEG on the surface of the nanoparticles (*NP-L20*).

Figure 7 shows the blood concentration profile of PGE_1 after intravenous administration to rats. A previous study using ^{3}H-labelled PGE_1 showed that PGE_1 was rapidly metabolized to 13,14-dihydro-15-keto-PGE_1 and that intact PGE_1 in plasma was only about 3% of the injected dose at 20 seconds after administration of Lipo-PGE_1 (40). In agreement with that result, PGE_1 was not detected by enzyme immunoassay even at 5 min after administration of Lipo-PGE_1, indicating that it leaked out from Lipo-PGE_1 into the circulation because of limited stability. After PGE_1CD (PGE_1 clathrated in cyclodextrin) was administered, there was also rapid clearance of PGE_1 due to extremely weak interaction with cyclodextrin in the blood. On the other hand, an extended residence time of PGE_1 in the blood was observed after nanoparticles (*NP-L33, -L20* , and *-L20s*) were administered (Fig. 7). Some pharmacokinetic parameters clearly displayed a significant difference between the nanoparticles and Lipo-PGE_1 (Table II). Prolonged residence of PGE_1 in the blood was based on two significant effects, which were protection of PGE_1 from

Table II. Comparative Pharmacokinetic Parameters of Various PGE_1 Formulations

	NP-L33	NP-L20	NP-L20s	NP-DL18	Lipo-PGE_1	PGE_1CD
$T_{1/2}$(h)	10.9±0.6	10.2±0.2	14.8±2.1	6.0±0.7	<0.08	<0.08
AUC_∞($\mu g\,h/ml$)	21.2±1.7	18.6±4.6	21.9±1.8	8.5±1.1	<0.07	<0.07
CL (ml/h kg)	6.3±0.5	7.5±2.1	6.1±0.5	15.8±2.1	>2,000	>2,000

The parameters were calculated based on the results shown in Fig. 7.
$t_{1/2}$ half-life, AUC_∞ area under the curve, CL total body clearance

inactivation in the lungs due to stable incorporation in the nanoparticles, and reduced interaction between the nanoparticles and cells of the MPS. When the nanoparticles were prepared from PDLLA (*NP-DL18*), PGE_1 was cleared from the blood faster than when the particles were prepared from PLLA (*NP-L33, -L20,* and *-L20s*), indicating more rapid PGE_1 release from PDLLA nanoparticles as shown in Fig. 5. Although the size of nanoparticles, as well as their surface properties, is usually an important factor in prolonging their circulation, the PLLA nanoparticles (*NP-L20*; 117nm and *NP-L20s*; 71nm) evaluated in this study exhibited little difference of residence times (Table II). Therefore, *NP-L20* with a higher PGE_1 content was used for the subsequent studies.

Longer residence of PGE_1 may not only enhance its therapeutic effects but also side effects, while rapid inactivation of PGE_1 with conventional therapeutic strategies abolishes both. However, preferential accumulation in target lesions should lead to enhancement of the therapeutic effect with minimal systemic side effects. In a rat model of peripheral vascular disease, preferential accumulation of the nanoparticles in right hind paw was observed at 1day after administration (Fig. 8), probably due to an EPR effect on circulating nanoparticles (18–20). Taken together, these results strongly suggest that nanoparticles coated with PEG may be useful for the treatment of vascular disorders such as chronic arteriosclerosis obliterans and vibration disease.

In addition, this technique for achieving the stable retention of PGE_1 in solid particles may help to advance various clinical applications of PGE_1. As shown in Fig. 6, uncoated nanoparticles were rapidly internalized by cells of the MPS. Such uncoated nanoparticles generally exhibited much higher accumulation in the liver after intravenous administration due to uptake by cells of the MPS such as Kupffer cells. Therefore, uncoated nanoparticles may be useful for the treatment of hepatopathy, fulminant viral hepatitis, and primary graft nonfunction, or for the promotion of liver regeneration. Apart from the intravenous administration of solid particles, local administration may also provide an advanced therapeutic effect. The utility of larger PLGA/PLA particles such as microspheres and implants for the control of drug release *in vivo* has been well established (21–23). Thus, local injection of such larger solid particles incorporating PGE_1 may lead to a long-term therapeutic effect at a limited location.

Finally, nanoparticles (*NP-L20*) could be successfully prepared on a large scale (30-fold scale), sterilized by filtration using a 0.2 μm membrane filter, and freeze-dried in the presence of sucrose. During storage of the freeze-dried nanoparticles for 6 months at 4°C, no chemical changes of PGE_1 or leaking (burst release) from the nanoparticles were observed. Concerning safety for clinical use, the additives in the nanoparticle formulations seem to be acceptable. PLA and PEG-PLA are desirable materials as excipients, because both are biodegradable and biocompatible, show low immunogenicity, and have little toxicity (41,42). Furthermore, iron is known to be one of the less toxic metals and some MRI contrast agents (such as Feridex® and Resovist®) with a high iron content are already being used clinically. The organic solvents that were employed (acetone and 1,4-dioxane) are harmful, but the residual content of such solvents in the nanoparticles could be decreased by ultrafiltration and freeze-drying. The residual level of solvents was sufficiently low according to the Guideline for Residual Solvents (ICH Harmonised Tripartite Guideline). Overall, our results suggest the utility of nanoparticles for various clinical applications.

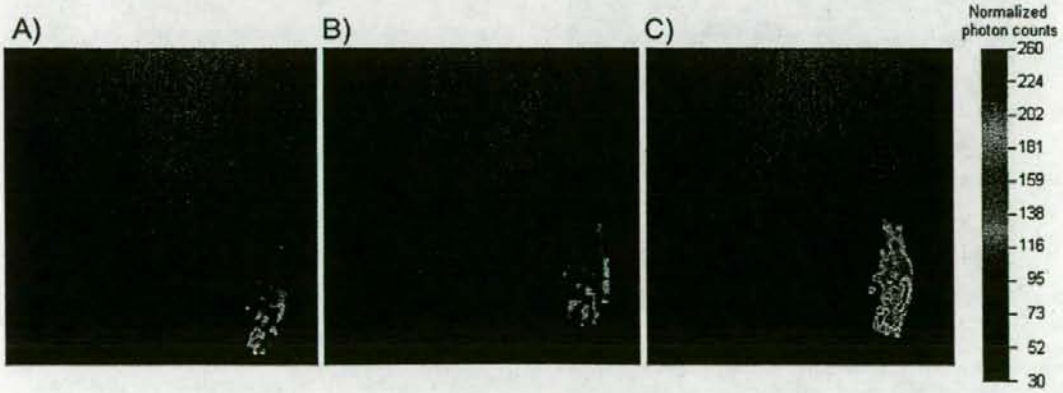

Fig. 8. Accumulation of nanoparticles containing Cy7 dye in the right hind paw in a rat model of peripheral vascular disease. Images were obtained at 1 day after intravenous administration of **A** Cy7 monomer, **B** Cy7-loaded Lipo-PGE_1, or (**C**) Cy7-loaded nanoparticles (*NP-L20* in Table I). The color bar indicates normalized photon counts derived from Cy7.

CONCLUSIONS

In conclusion, nanoparticles that efficiently incorporated PGE_1 were developed by blending PLA homopolymers and PEG-PLA block copolymers in the presence of iron. The stable retention of PGE_1 by the nanoparticles provided protection against its inactivation in the lungs, and sustained PGE_1 release could be obtained depending on the isomers and molecular weight of the PLA homopolymers. Coating of nanoparticles with PEG facilitated their accumulation in vascular lesions, suggesting the potential clinical application of nanoparticles for vascular disorders instead of Lipo-PGE_1. Use of this strategy to prolong the *in vivo* residence time and control the biodistribution of PGE_1 may open up various opportunities for clinical application.

ACKNOWLEDGEMENTS

We thank Sachiyo Shibata, Tetsushi Kubota and Yukie Tokura for their assistance with the animal experiments.

REFERENCES

1. D. M. Kerins, R. Murray, and G. A. FitzGerald. Prostacyclin and prostaglandin E1: molecular mechanisms and therapeutic utility. *Prog. Hemost. Thromb.* **10**:307–337 (1991).
2. A. Creutzig and L. Caspary. Prostanoids in therapy of peripheral arterial occlusive disease. *Therapie* **46**:241–245 (1991).
3. M. Golub, P. Zia, M. Matsuno, and R. Horton. Metabolism of prostaglandins A1 and E1 in man. *J. Clin. Invest.* **56**:1404–1410 (1975).
4. M. Bygdeman. Pharmacokinetics of prostaglandins. *Best Pract. Res. Clin. Obstet Gynaecol.* **17**:707–716 (2003).
5. G. Bianchi Porro and F. Parente. Side effects of anti-ulcer prostaglandins: an overview of the worldwide clinical experience. *Scand. J. Gastroenterol.* **24**:224–229 (1989).
6. G. Holló. The side effects of the prostaglandin analogues. *Expert Opin. Drug Saf.* **6**:45–52 (2007).
7. Y. Mizushima, A. Yanagawa, and K. Hoshi. Prostaglandin E1 is more effective, when incorporated in lipid microspheres, for treatment of peripheral vascular diseases in man. *J. Pharm. Pharmacol.* **35**:666–667 (1983).
8. Y. Mizushima. Lipo-prostaglandin preparations. *Prostaglandins Leukot. Essent. Fatty Acids* **42**:1–6 (1991).
9. T. Yamaguchi and Y. Mizushima. Lipid microspheres for drug delivery from the pharmaceutical viewpoint. *Crit. Rev. Ther. Drug Carrier Syst.* **11**:215–229 (1994).
10. D. F. Eierman, M. Yagami, S. M. Erme, S. R. Minchey, P. A. Harmon, K. J. Pratt, and A. S. Janoff. Endogenously opsonized particles divert prostanoid action from lethal to protective in models of experimental endotoxemia. *Proc. Natl. Acad. Sci. U S A* **92**:2815–2819 (1995).
11. S. Feld, G. Li, J. Amirian, P. Felli, W. K. Vaughn, M. Accad, T. R. Tolleson, C. Swenson, M. Ostro, and R. W. Smalling. Enhanced thrombolysis, reduced coronary reocclusion and limitation of infarct size with liposomal prostaglandin E1 in a canine thrombolysis model. *J. Am. Coll. Cardiol.* **24**:1382–1390 (1994).
12. H. Pan, P. Kopecková, J. Liu, D. Wang, S. C. Miller, and J. Kopecek. Stability in plasmas of various species of HPMA copolymer-PGE(1) conjugates. *Pharm Res.* **24**:2270–2280 (2007).
13. K. Akamatsu, Y. Yamasaki, M. Nishikawa, Y. Takakura, and M. Hashida. Synthesis and pharmacological activity of a novel water-soluble hepatocyte-specific polymeric prodrug of prostaglandin E(1) using lactosylated poly(L-glutamic hydrazide) as a carrier. *Biochem. Pharmacol.* **62**:1531–1536 (2001).
14. Y. Mizushima, T. Hamano, S. Haramoto, S. Kiyokawa, A. Yanagawa, K. Nakura, M. Shintome, and M. Watanabe. Distribution of lipid microspheres incorporating prostaglandin E1 to vascular lesions. *Prostaglandins Leukot. Essent. Fatty Acids* **41**:269–272 (1990).
15. S. Kawakami, C. Munakata, S. Fumoto, F. Yamashita, and M. Hashida. Targeted delivery of prostaglandin E1 to hepatocytes using galactosylated liposomes. *J. Drug Target.* **8**:137–142 (2000).
16. R. Igarashi, Y. Mizushima, M. Takenaga, K. Matsumoto, Y. Morizawa, and A. Yasuda. A stable PGE1 prodrug for targeting therapy. *J. Control. Release* **20**:37–46 (1992).
17. C. E. Astete and C. M. Sabliov. Synthesis and characterization of PLGA nanoparticles. *J. Biomater. Sci. Polym. Ed.* **17**:247–289 (2006).
18. R. Gref, Y. Minamitake, M. T. Peracchia, V. Trubetskoy, V. Torchilin, and R. Langer. Biodegradable long-circulating polymeric nanospheres. *Science* **263**:1600–1603 (1994).
19. H. Maeda, J. Wu, T. Sawa, Y. Matsumura, and K. Hori. Tumor vascular permeability and the EPR effect in macromolecular therapeutics: a review. *J. Control. Release* **65**:271–284 (2000).
20. K. Avgoustakis. Pegylated poly(lactide) and poly(lactide-co-glycolide) nanoparticles: preparation, properties and possible applications in drug delivery. *Curr. Drug Deliv.* **1**:321–333 (2004).
21. S. J. Douglas, S. S. Davis, and L. Illum. Nanoparticles in drug delivery. *Crit. Rev. Ther. Drug Carrier Syst.* **3**:233–261 (1987).
22. H. Okada and H. Toguchi. Biodegradable microspheres in drug delivery. *Crit. Rev. Ther. Drug Carrier Syst.* **12**:1–99 (1995).
23. C. E. Astete and C. M. Sabliov. Synthesis and characterization of PLGA nanoparticles. *J. Biomater. Sci. Polym. Ed.* **17**:247–289 (2006).
24. T. Ishihara, N. Izumo, M. Higaki, E. Shimada, T. Hagi, L. Mine, Y. Ogawa, and Y. Mizushima. Role of zinc in formulation of PLGA/PLA nanoparticles encapsulating betamethasone phosphate and its release profile. *J. Control. Release* **105**:68–76 (2005).
25. M. Higaki, T. Ishihara, N. Izumo, M. Takatsu, and Y. Mizushima. Treatment of experimental arthritis with poly(D, L-lactic/glycolic acid) nanoparticles encapsulating betamethasone sodium phosphate. *Ann. Rheum. Dis.* **64**:1132–1136 (2005).
26. E. Pişkin, X. Kaitian, E. B. Denkbaş, and Z. Küçükyavuz. Novel PDLLA/PEG copolymer micelles as drug carriers. *J. Biomater. Sci. Polym. Ed.* **7**:359–373 (1995).
27. T. Riley, S. Stolnik, C. R. Heald, C. D. Xiong, M. C. Garnett, L. Illum, and S. S. Davis. Physicochemical evaluation of nanoparticles assembled from poly(lactic acid)-poly(ethylene glycol) (PLA-PEG) block copolymers as drug delivery vehicles. *Langmuir* **17**:3168–3174 (2001).
28. S. Kamei, Y. Inoue, H. Okada, M. Yamada, Y. Ogawa, and H. Toguchi. New method for analysis of biodegradable polyesters by high-performance liquid chromatography after alkali hydrolysis. *Biomaterials* **13**:953–958 (1992).
29. S. Ashida, M. Ishihara, H. Ogawa, and Y. Abiko. Protective effect of ticlopidine on experimentally induced peripheral arterial occlusive disease in rats. *Thromb Res.* **18**:55–67 (1980).
30. H. Hara, H. Shimada, A. Kitajima, and Y. Tamao. Effect of (+/−)-2-(dimethylamino)-1-[[o-(m-methoxyphenethyl)phenoxy] methyl]ethyl hydrogen succinate on experimental models of peripheral obstructive disease. *Arzneimittelforschung* **41**:616–620 (1991).
31. C. M. Flynn. Hydrolysis of inorganic iron(III) salts. *Chem. Rev.* **84**:31–41 (1984).
32. T. Liu and E. S. Chian. Effect of base addition rate on the preparation of partially neutralized ferric chloride solutions. *J. Colloid Interface Sci.* **284**:542–547 (2005).
33. L. Weiss and J. R. Subjeck. The densities of colloidal iron hydroxide particles bound to microvilli and the spaces between them: studies on glutaraldehyde-fixed ehrlich ascites tumor cells. *J. Cell Sci.* **14**:215–223 (1974).
34. G. A. Parks. The isoelectric points of solid oxides, solid hydroxides, and aqueous hyrdoxo complex systems. *Chem. Rev.* **65**:177–198 (1965).
35. H. Murakami, M. Kobayashi, H. Takeuchi, and Y. Kawashima. Preparation of poly(DL-lactide-co-glycolide) nanoparticles by modified spontaneous emulsification solvent diffusion method. *Int. J. Pharm.* **187**:143–52 (1999).
36. Y. Dong and S. S. Feng. Nanoparticles of poly(D,L-lactide)/methoxy poly(ethylene glycol)-poly(D,L-lactide) blends for con-

trolled release of paclitaxel. *J. Biomed. Materials Res. A.* **78**:12–19 (2006).
37. H. Okada, M. Yamamoto, T. Heya, Y. Inoue, S. Kamei, Y. Ogawa, and H. Toguchi. Drug delivery using biodegradable microspheres. *J. Control. Release* **28**:121–129 (1994).
38. R. Jalil and J. R. Nixon. Biodegradable poly(lactic acid) and poly (lactide-co-glycolide) microcapsules: problems associated with preparative techniques and release properties. *J. Microencapsul.* **7**:297–325 (1990).
39. V. C. Mosqueira, P. Legrand, J. L. Morgat, M. Vert, E. Mysiakine, R. Gref, J. P. Devissaguet, and G. Barratt. Biodistribution of long-circulating PEG-grafted nanocapsules in mice: effects of PEG chain length and density. *Pharm Res.* **18**:1411–1419 (2001).
40. Clinical report (Kiso to Rinsho). **20**:4399–4428 (1986). (written in Japanese)
41. M. S. Shive and J. M. Anderson. Biodegradation and biocompatibility of PLA and PLGA microspheres. *Adv. Drug Deliv. Rev.* **28**:5–24 (1997).
42. J. P. Plard and D. Bazile. Comparison of the safety profiles of PLA50 and Me.PEG-PLA50 nanoparticles after single dose intravenous administration to rat. *Colloids Surf. B biointerfaces* **16**:173–183 (1999).

Carcinogenesis vol.29 no.10 pp.1994–2000, 2008
doi:10.1093/carcin/bgn134
Advance Access publication June 26, 2008

NSAIDs suppress the expression of claudin-2 to promote invasion activity of cancer cells

Shinji Mima, Masaya Takehara, Hiroko Takada, Tomoko Nishimura, Tatsuya Hoshino and Tohru Mizushima*

Graduate School of Medical and Pharmaceutical Sciences, Kumamoto University, Kumamoto 862-0973, Japan

*To whom correspondence should be addressed. Tel/Fax: +81 96 371 4323; Email: mizu@gpo.kumamoto-u.ac.jp

Non-steroidal anti-inflammatory drugs (NSAIDs) show chemopreventive effects; however, the precise molecular mechanism of these effects is still unclear. On the other hand, the expression of proteins that form tight junctions (TJs) (such as claudins) in clinically isolated tumors is frequently altered relative to normal tissue. We previously reported that NSAIDs upregulate the expression of claudin-4 and that this upregulation contributes to NSAID-dependent inhibition of both migration activity and anchorage-independent growth of cancer cells. In the current study, we have systematically examined the effects of various NSAIDs on the expression of various TJ proteins and have found that NSAIDs specifically and drastically inhibit the expression of claudin-2. Overexpression or suppression of claudin-2 expression caused stimulation or inhibition, respectively, of the invasion and migration activity of cancer cells. Furthermore, NSAIDs inhibited the invasion and migration activity of cancer cells and this inhibition was suppressed by overexpression of claudin-2. In contrast, neither cell growth nor apoptosis induced by lack of anchorage of cancer cells was affected by overexpression or suppression of expression of claudin-2. These results suggest that inhibition of claudin-2 expression by NSAIDs contributes to NSAID-dependent inhibition of invasion of cancer cells *in vitro* and that it may be involved in the chemopreventive effects of NSAIDs by inhibiting metastasis *in vivo*.

Introduction

Non-steroidal anti-inflammatory drugs (NSAIDs) are useful drugs for alleviating pain, fever and inflammation. The anti-inflammatory action of NSAIDs is mediated via their inhibitory effect on cyclooxygenase (COX) activity and synthesis of prostaglandins (PGs), which have a strong capacity to induce inflammation. A range of epidemiological studies have revealed that prolonged NSAID use reduces the risk of cancer, whereas preclinical and clinical studies have indicated that some NSAIDs are effective in the treatment and prevention of cancer (1). Because the antitumor activity of NSAIDs is potent and the safety of longtime use of NSAIDs has been proven by a vast amount of clinical data, NSAIDs have attracted considerable attention as a new type of antitumor drug. In the USA, the Food and Drug Administration has approved the use of celecoxib, an NSAID, for the treatment of familial adenomatous polyposis.

PGs, such as PGE_2, inhibit apoptosis of cancer cells and stimulate growth and invasion of cancer cells and angiogenesis (2–4). Furthermore, overexpression of COX-2 (a subtype of COX) in various tumor cells and tissues has been reported (5,6). Therefore, it was believed that the antitumor effect of NSAIDs is mediated only through the inhibition of COX. However, several lines of evidence suggest that the antitumor effect of NSAIDs also involves a COX-independent mechanism (7,8). In order to reveal the nature of this COX-independent mechanism, we systematically searched for genes whose expression is upregulated by indomethacin (an NSAID) in a COX-independent manner in human gastric carcinoma (AGS) cells. This study has revealed that expression of some genes encoding tight junction (TJ) proteins (claudin-4, claudin-1 and occludin) is induced by indomethacin (9).

TJs are the most apical intercellular structures in epithelial and endothelial cells and create a physiological barrier separating the apical and basolateral spaces. TJs contain transmembrane proteins such as occludin and the claudins, whose C-terminal regions interact with cytosolic proteins, such as zonula occludens-1 (10,11). TJs have attracted considerable attention in relation to tumor progression because a loss of TJ structure and function is frequently observed in epithelium-derived cancers (12). This loss of TJ structure and function is though to promote cancer progression through allowing constitutive accessibility of cancers to nutrients and growth factors (13) and other mechanism. Furthermore, alteration of expression of the proteins that constitute TJs, especially claudins has been shown to modulate various cell functions related to tumor progression *in vitro* (12,13). For example, we recently reported that overexpression of claudin-4 or suppression of expression of claudin-4 caused a decrease or an increase, respectively, in the anchorage-independent growth and migration activity of AGS cells (9). Studies from other groups have also shown that alterations to the expression of claudins (claudin-1, -3, -4, -5) affect the invasion and migration activities and anchorage-independent growth of cancer cells (14–18). However, the effect of expression of other claudins, including claudin-2, on cell functions related to cancer progression has remained unknown. Among the claudins, claudin-2 is unique because its expression increases the paracellular permeability of some molecules [in other words claudin-2 decreases the function of TJs (19,20)] and its messenger RNA (mRNA) expression is regulated by various mechanisms (21–23).

Based on the observations described above, it is reasonable to hypothesize that NSAIDs achieve their antitumor activity by altering the expression of TJ proteins. In fact, we previously reported that induction of expression of claudin-4 by NSAIDs contributes to NSAID-dependent inhibition of both migration and anchorage-independent growth of cancer cells (9). In this study, we examined the effects of various NSAIDs on the expression of various TJ proteins in AGS cells and found that NSAIDs inhibit the expression of claudin-2 specifically and extensively. Experiments using an overexpression plasmid and small interfering RNA (siRNA) revealed that expression of claudin-2 increases the invasion and migration activity of AGS cells and suggests that NSAID-dependent inhibition of the invasion and migration activity of AGS cells is due to the NSAID-dependent downregulation of claudin-2 expression. We suggest that NSAIDs positively or negatively affect the expression of claudins, depending on the claudin species, and that this action plays an important role in conferring the chemopreventive effect of NSAIDs through inhibition of metastasis.

Materials and methods

Chemicals and media

Ham F12, Dulbecco's modified Eagle's medium and RPMI1640 medium were obtained from Nissui Pharmaceutical Co (Tokyo, Japan). HilyMax and 1,2-bis(2-aminophenoxy)ethane-*N,N,N′N′*-tetraacetic acid (BAPTA-AM) were obtained from Dojindo Co (Kumamoto, Japan). Fetal bovine serum (FBS), fibronectin, G418, 3-(4, 5-dimethyl-thiazol-2-yl)-2, 5-diphenyl tetrazolium bromide and diclofenac were obtained from Sigma Co (Tokyo, Japan). Indomethacin was from Wako Co (Osaka, Japan). Celecoxib was obtained from LKT Laboratories (St. Paul, Minnesota). The plasmid psiRNA-h7SKneo was from InvivoGen (San Diego, California) and pcDNA3.1(−) and Lipofectamine (TM2000) were from Invitrogen (Tokyo, Japan). The RNeasy kit was obtained from Qiagen (Tokyo, Japan), first-strand complementary DNA (cDNA) synthesis kit was from GE Healthcare (Tokyo, Japan) and iQ SYBR Green Supermix was from Bio-Rad (Tokyo, Japan). Matrigel was from BD Biosciences

Abbreviations: BAPTA-AM, 1,2-bis(2-aminophenoxy)ethane-*N,N,N′N′*-tetraacetic acid; cDNA, complementary DNA; COX, cyclooxygenase; FBS, fetal bovine serum; MMP, matrix metalloproteinase; mRNA, messenger RNA; NSAID, non-steroidal anti-inflammatory drug; PCR, polymerase chain reaction; PG, prostaglandin; siRNA, small interfering RNA; TJ, tight junction.

(Tokyo, Japan) and the 24-well transwells were from Costar. Antibody against claudin-2 was from Zymed (San Francisco, California) and those against claudin-4 and actin were from Santa Cruz Biotechnology (Sata Cruz, California).

Cell culture and stimulation or suppression of claudin-2 expression

AGS and KATO-III cells (human carcinoma cell lines derived from stomach) were cultured in RPMI1640 medium containing 10% FBS and T-84 (human colonic adenocarcinoma cell line) and A549 (human lung adenocarcinoma) cells were cultured in Ham F12/Dulbecco's modified Eagle's medium containing 5% FBS. Cells (2×10^5 cells per well in a 24-well plate) were cultured for 24 h and then used in the experiments. Cell viability was determined by the 3-(4, 5-dimethyl-thiazol-2-yl)-2, 5-diphenyl tetrazolium bromide method as described previously (24).

A full-length human *CLDN2* cDNA was polymerase chain reaction (PCR) amplified from AGS cell cDNA and cloned into pcDNA3.1(−) to create the plasmid for overexpression of claudin-2.

We used the siRNA sequence of 5′-ACCTCGGATCCTACGGGACTTCTACTTCAAGAGAGTAGAAGTCCCGTAGGATCCTT-3′ as annealed oligonucleotides for repressing claudin-2 expression. A DNA fragment encoding this siRNA was cloned into a psiRNA-h7SKneo to create the plasmid for expression of this siRNA.

Transfection of AGS cells with plasmids was carried out using Lipofectamine (TM2000) or HilyMax according to the manufacturer's protocols. The stable transfectants expressing claudin-2 or siRNA for claudin-2 were selected by immunoblotting analysis. Positive clones were maintained in the presence of 300 μg/ml G418.

Real-time reverse transcription–PCR

Total RNA was extracted using an RNeasy kit according to the manufacturer's protocol. Samples (2.5 μg RNA) were reverse transcribed using a first-strand cDNA synthesis kit according to the manufacturer's instructions. Synthesized cDNA was used in real-time reverse transcription–PCR [Chromo 4 instrument (Bio-Rad)] experiments using iQ SYBR GREEN Supermix and analyzed with Opticon Monitor Software according to the manufacturer's instructions. The real-time PCR cycle conditions were 2 min at 50°C, followed by 10 min at 90°C and finally 45 cycles of 95°C for 30 s and 63°C for 60 s. Specificity was confirmed by electrophoretic analysis of the reaction products and by inclusion of template- or reverse transcriptase-free controls. To normalize the amount of total RNA present in each reaction, the *actin* cDNA was used as an internal standard.

Immunoblotting analysis

Membrane fractions were prepared as described previously (25). The protein concentration of the sample was determined by the Bradford method. Samples were applied to 12% polyacrylamide gels containing sodium dodecyl sulfate, subjected to electrophoresis, and proteins were then immunoblotted with each antibody.

Anoikis induction

Anoikis induction was assayed as described (26), with some modifications. Dishes were coated with 1% agarose to prevent cells from adhering to the plastic cell culture dishes. Solidified agarose was equilibrated and overlaid with Dulbecco's modified Eagle's medium supplemented with 10% FBS. After treatment with trypsin, cells were applied to these plates and rotated horizontally several times to allow the cells to form spheroidal aggregations. After incubation for 7 days, cells were collected, applied to normal cell culture dishes and the number of colonies derived from viable cells was counted after incubation for 3 days.

Invasion assay

The invasion assay was done as described previously (27), with some modifications. Serum-free RPMI1640 medium containing 5 mg/ml matrigel was applied to the upper chamber of a 24-well transwell and incubated at 37°C for 4 h. Cell suspension was applied to the matrigel and the lower chamber of the transwell was filled with culture media containing 10% FBS and 5 μg/ml fibronectin. The plate was incubated at 37°C for 24 h. Cells were removed from the upper surface of the membrane and the lower surface of the membrane was stained for 10 min with 0.5% crystal violet in 25% methanol, rinsed with distilled water and air-dried overnight. The crystal violet was then extracted with 0.1 M sodium citrate in 50% ethanol and the absorbance was measured at 585 nm.

Cell migration assays

In vitro wound healing assays were used to assess cell migration as described previously (9,28). Confluent AGS cells on a 24-well plate were used for this assay. Two linear wounds were made with a p200 pipette tip. The cell-free area was measured before and after a 24 h incubation (healing step) by use of Scion Image software (Scion Corporation, Frederick, Maryland).

Statistical analysis

All values are expressed as the mean ± SEM. Two-way analysis of variance, followed by the Tukey test or the Student's *t*-test for unpaired results, was used to evaluate differences between more than three groups or between two groups, respectively. Differences were considered to be significant for values of $P < 0.05$.

Results

Effect of NSAIDs on expression of claudins

We used a real-time reverse transcription–PCR technique to examine the effect of various NSAIDs on expression of claudins and other TJ proteins in AGS cells. First, we examined the effect of various NSAIDs on cell viability and determined the concentration of each NSAID required to reduce cell viability to 70% (0.35 mM indomethacin, 30 μM celecoxib, 0.2 mM diclofenac, 5 mM aspirin, 1 mM ibuprofen and 0.18 mM nimesulid). We next examined the effects of these concentrations of NSAIDs on mRNA expression of various TJ proteins (Table I). The mRNA expression of *CLDN4* was clearly upregulated by all NSAIDs tested and that of *CLDN1* and *occludin* was slightly upregulated, as described previously (9). Of all the proteins tested, a characteristic feature in response to the NSAIDs was identified for claudin-2: all of the NSAIDs tested suppressed the mRNA expression of *CLDN2* and the extent of the suppression was more distinct than for other claudins (Table I). The mRNA expression of *CLDN7* and *zonula occludens* or *CLDN3*, *CLDN5* and *CLDN6* showed a tendency to be increased or decreased, respectively, by NSAIDs. However, for these genes, the changes in expression were not observed in response to some NSAIDs and the extent of the changes were not as distinct as was observed for *CLDN4* and *CLDN2* (Table I). COX exists as two subtypes, COX-1 and COX-2. Celecoxib

Table I. Alteration of mRNA expression of TJ-related genes by NSAIDs

	IND	CEL	DIC	ASP	IBU	NIM
CLDN1	1.43	1.64	1.43	1.24	2.16	1.75
CLDN2	0.01	0.48	0.12	0.01	0.03	0.09
CLDN3	0.47	1.78	0.99	0.51	0.59	0.84
CLDN4	2.37	1.51	2.45	3.95	4.42	2.89
CLDN5	0.57	0.76	0.19	0.18	0.47	1.92
CLDN6	0.73	0.86	0.98	1.00	0.74	0.86
CLDN7	1.45	1.75	1.42	1.26	2.03	1.37
Occludin	1.35	1.06	1.32	1.53	1.83	1.01
Zonula occludens-1	2.10	1.86	1.77	0.86	1.64	1.53

AGS cells were incubated with 0.35 mM indomethacin (IND), 30 μM celecoxib (CEL), 0.2 mM diclofenac (DIC), 5 mM aspirin (ASP), 1 mM ibuprofen (IBU) or 0.18 mM nimesulid (NIM) for 24 h and total RNA was extracted. Samples were subjected to real-time reverse transcription–PCR using a specific primer set for each gene. Values were normalized to *actin* expression and expressed relative to the control sample (i.e. without NSAID control). We performed real-time RT–PCR experiments twice on each cDNA and showed the mean of them.